A&A 586, A155 (2016)
DOI: 10.1051/0004-6361/201527161

Astronomy & Astrophysics

Absolute magnitudes and phase coefficients of trans-Neptunian objects

A. Alvarez-Candal[1], N. Pinilla-Alonso[2], J. L. Ortiz[3], R. Duffard[3], N. Morales[3], P. Santos-Sanz[3], A. Thirouin[4], and J. S. Silva[1]

[1] Observatório Nacional / MCTI, Rua General José Cristino 77, 20921-400 Rio de Janeiro, RJ, Brazil
e-mail: alvarez@on.br
[2] Department of Earth and Planetary Sciences, University of Tennessee, Knoxville, TN, 37996, USA
[3] Instituto de Astrofísica de Andalucía, CSIC, Apt 3004, 18080 Granada, Spain
[4] Lowell Observatory, 1400 W Mars Hill Rd, Flagstaff, 86001 Arizona, USA

Received 10 August 2015 / Accepted 27 November 2015

ABSTRACT

Context. Accurate measurements of diameters of trans-Neptunian objects (TNOs) are extremely difficult to obtain. Thermal modeling can provide good results, but accurate absolute magnitudes are needed to constrain the thermal models and derive diameters and geometric albedos. The absolute magnitude, H_V, is defined as the magnitude of the object reduced to unit helio- and geocentric distances and a zero solar phase angle and is determined using phase curves. Phase coefficients can also be obtained from phase curves. These are related to surface properties, but only few are known.
Aims. Our objective is to measure accurate V-band absolute magnitudes and phase coefficients for a sample of TNOs, many of which have been observed and modeled within the program "TNOs are cool", which is one of the *Herschel* Space Observatory key projects.
Methods. We observed 56 objects using the V and R filters. These data, along with those available in the literature, were used to obtain phase curves and measure V-band absolute magnitudes and phase coefficients by assuming a linear trend of the phase curves and considering a magnitude variability that is due to the rotational light-curve.
Results. We obtained 237 new magnitudes for the 56 objects, six of which were without previously reported measurements. Including the data from the literature, we report a total of 110 absolute magnitudes with their respective phase coefficients. The average value of H_V is 6.39, bracketed by a minimum of 14.60 and a maximum of −1.12. For the phase coefficients we report a median value of 0.10 mag per degree and a very large dispersion, ranging from −0.88 up to 1.35 mag per degree.

Key words. methods: observational – techniques: photometric – Kuiper belt: general

1. Introduction

The phase curve of a minor body shows how the reduced magnitude[1] of the body changes with phase angle. The phase angle, α, is defined as the angle measured at the location of the body that Earth and the Sun subtend. These curves show a complex behavior: for phase angles between 5°and 30° they follow an overall linear trend, while at small angles a departure from linearity often occurs. In 1956 T. Gehrels coined the expression "opposition effect" and attributed it to the sudden increase of brightness at small α shown in the phase curve of asteroid 20 Massalia (Gehrels 1956), although no explanation was offered. Since then, many works have modeled phase curves, with or without opposition effect, analyzing the relationship between these curves and the properties of the surface: particle sizes, scattering properties, albedos, compaction, or composition, either by using astronomical or laboratory data or theoretical modeling (e.g., Hapke 1963; Bowell et al. 1989; Nelson et al. 2000; Shkuratov et al. 2002 and references therein).

In addition to providing information about surface properties, phase curves are also important because by using them, we can measure the absolute magnitude, H, of an airless body. H is defined as the reduced magnitude of an object at $\alpha = 0°$. Moreover, H is related to the diameter of the body, D, and its geometric albedo p. For magnitudes in the V band,

$$D\,[\mathrm{km}] = 1.324 \times \frac{10^{(3-H_V/5)}}{\sqrt{p_V}}. \quad (1)$$

The first minor bodies with measured phase curves were asteroids (for instance, the aforementioned work by Gehrels in 1956). Today, we know that low-albedo (taxonomic classes D, P, or C) asteroids show lower opposition effect spikes than higher albedo asteroids (S or M asteroids; Belsakya & Shevchenko 2000). Modern technologies have also allowed us to obtain incredible data of a handful of objects. Examples are the recent work on comet 67P/Churyumov-Gerasimenko by Fornasier et al. (2015), which used data from the ROSETTA spacecraft, or huge databases, such as the 250 000 absolute magnitudes of asteroids presented by Vereš et al. (2015) from Pan-STARRS.

Unfortunately, such data are not yet available for objects farther away in the solar system, with the exception of 134340 Pluto. Therefore, many of the physical characteristic of the trans-Neptunian population, for instance, size, albedo, or density, are still hidden from us because of the limited

[1] The observed standard magnitude normalized to the distance of the Sun and Earth.

quality of the information we can currently obtain: visible and/or near-infrared spectroscopy of about 100 objects (Barucci et al. 2011, and references therein), and colors of about 300 (Hainaut et al. 2012) drawn from a known population of more than 1400 objects. Moreover, these data belong to the largest known trans-Neptunian objects (TNOs), the most easily observed ones, or some Centaurs. These last are a population of dynamically unstable objects whose orbits cross those of the giant planets; they are considered to come from the trans-Neptunian region and therefore to be representative of this population. Nevertheless, considerable progress has been made in understanding the dynamical structure of the region, but the bulk of the physical characteristics of the bodies that inhabit it remains poorly determined. Several observational studies conducted in the past years show a vast heterogeneity in physical and chemical properties.

With the objective of enlarging our knowledge of the TNO population, The *Herschel* open time key program on TNOs and Centaurs: "TNOs are cool" (Müller et al. 2007) was granted with 372.7 h of observation on the *Herschel* Space Observatory (HSO). The observations are complete with a sample of 130 observed objects. The observed data are fed into thermal models (Müller et al. 2010), where a series of free parameters are fitted; among them are p_V and D. These two quantities could be constrained using ground-based data and thus fixing at least one of them in the modeling, which improves the accuracy of the results. Several of the targets observed with *Herschel* do not have a reliable H_V magnitude, which is fundamental to compute D and p_V (i.e., small uncertainties in H_V mean smaller uncertainties in D and p_V).

To supply this, the HSO program "TNOs are cool" needs support observations from ground-based telescopes.

One critical problem that arises when studying phase curves of TNOs is the fact that α can only attain low values for observations made from Earth-based facilities. For comparison: a typical main-belt asteroid can be observed up to 20° or 30°, while a typical TNO can only reach up to 2°. This means that for TNOs, we are observing well within the opposition effect region, which prevents us from using the full power of photometric models. On the other hand, the phase curves are very well approximated by linear functions within this restricted phase angle region (e.g., Sheppard & Jewitt 2002). Some efforts have been made in this direction (see review by Belskaya et al. 2008, or the recent works by Perna et al. 2013; and Böhnhardt et al. 2014), but most of them used limited samples (usually one observation) and assumed average values of the phase coefficients.

With this in mind, we started a survey with various telescopes to obtain V and R magnitudes for several TNOs at as many different phase angles as possible to measure phase curves and through them determine H_V. The survey is being carried out in both hemispheres using telescopes at different locations. In the next section we describe the observations and the facilities where the data were obtained. In Sect. 3 we present the results, while their analysis is presented in Sect. 4. The discussion and some conclusions obtained from this work are presented in Sect. 5.

2. Observations and data reduction

The data we present here were collected during several observing runs between September 2011 and July 2015 for well over 40 nights. The instruments and facilities used were the Calar Alto Faint Object Spectrograph at the 2.2 m telescope, CAHA2.2, and the Multi Object Spectrograph for Calar Alto at the 3.5 m telescope, CAHA3.5, of the Calar Alto Observatory[2], which is located at the Sierra de Los Filabres (Spain); the Wide Field Camera at the 2.5 m *Isaac Newton* Telescope (INT), located at the Roque de los Muchachos Observatory[3] (Spain); the direct camera at the 1.5 m telescope, OSN, of the Sierra Nevada Observatory[4] (Spain); the SOAR Optical Imager at the 4.1 m Southern Astrophysical Research telescope[5] located at Cerro Pachón (Chile); the direct camera at the 1 m telescope of the Observatório Astronômico do Sertão de Itaparica[6], OASI, Brazil; and the optical imaging component of the Infrared-Optical suite of instruments (IO:O) at the 2.0 m Liverpool telescope, Live, located at the Roque de los Muchachos Observatory[7] (Spain). Descriptions of instruments and telescopes can be found at their respective homepages.

We always attempted to observe using the V and R filters sequentially, but in some cases this was not possible, either because of deteriorating weather conditions (i.e., no observation was possible) or because of instrumental or telescope problems. The objects were targeted, whenever possible, at different phase angles, aiming at the widest spread possible. Along with the TNOs we targeted several standard star fields each night (from Landolt 1992; and Clem & Landolt 2013), or they were provided by the observatory, as in the case of the Liverpool telescope. We aimed at observing three different fields at three different airmasses per night to cover the range of airmasses of our main targets.

Most observations were carried out by observing the target during three exposures of 600 s per filter, although in some cases shorter exposures (300 or 400 s) were used to avoid saturation from nearby bright stars or trailing by faster objects (a Centaur can reach up to 2 arcsecs in 10 min). We did not use differential tracking. The combination of the different images allowed us to increase the signal-to-noise ratio while keeping trailing at reasonable values. We found this approach better than tracking at a non-sidereal rate for 1800 s, for instance, because we obtained a better removal of bad pixels, cosmic ray hits, or background sources during stacking of shorter exposures.

Data reduction was performed using standard photometric methods with IRAF. Master bias frames were created from daily files, as well as master flat fields in both filters. Files including TNOs and standard stars fields were bias- and flat-field calibrated. Data from the Liverpool telescope were provided already calibrated. For most of the objects, identification was straightforward by blinking different images or, in the most complicated cases, using Aladin[8] (Bonnarel et al. 2000). Instrumental apparent magnitudes were obtained using aperture photometry, for which we selected an aperture typically three times the seeing measured in the images for TNOs and standard stars. Whenever a TNO was too close to another source, either by poor observing timing or by crowded fields, we instead performed aperture correction (see Stetson 1990).

Using the standard stars, we computed extinction coefficients and color terms to correct the magnitudes of the TNOs thus

$$m_0 = m - \chi[k_1 + k_2(v - r)], \quad (2)$$

where m_0 is the apparent instrumental magnitude corrected by extinction (v_0 or r_0), m is the apparent instrumental

[2] http://www.caha.es
[3] http://www.ing.iac.es/Astronomy/telescopes/int/
[4] http://www.osn.iaa.es/content/15-m-telescope
[5] http://www.soartelescope.org/
[6] http://www.on.br/impacton/
[7] http://telescope.livjm.ac.uk/
[8] http://aladin.u-strasbg.fr/

magnitude (v or r), χ is the airmass, k_1 and k_2 are the zeroth- and first-order extinction coefficients, and $(v - r)$ is the apparent instrumental color of the TNO.

Next, we translated m_0 into the standard system. The transformation, to order zero, is

$$M = m_0 + ZP, \tag{3}$$

where M is the calibrated magnitude, and ZP is the zero point. We note that because we had many runs in the same telescopes, we computed average extinction coefficients for each site that were used whenever the data did not allow us to compute the night value. The same is true for ZPs. In the particular case of the Liverpool telescope, we used the average extinction coefficient for the Roque de los Muchachos observatory.

Table A.1 lists all observed objects, along with its calibrated V and R magnitudes, the night the object was observed, the heliocentric (r) and geocentric (Δ) distances, and the phase angle (α) at the moment of observation, the telescope used, and a series of notes indicating whether we used average extinction coefficients, average zero points, or if the object had no previously reported data.

The errors in the final magnitudes include (i) the error in the instrumental magnitudes, provided by IRAF (σ_i); (ii) the error due to atmospheric extintion, estimated as $\sigma_e = m_0 - (m - \chi k_1)$; and the error in the calibration to the standard system, σ_{ZP}. Therefore $\sigma^2 = \sigma_i^2 + \sigma_e^2 + \sigma_{ZP}^2$. Whenever aperture correction was performed, $\sigma_i^2 = \sigma_{i1}^2 + \sigma_{i2}^2$, where σ_{i1} is the error provided by IRAF within the smaller aperture and σ_{i2} is the error in the aperture correction, computed using the task `mkapfile` within IRAF.

3. Analysis

In total we obtained 237 new magnitudes for 56 objects, 6 of which did not have any magnitude reported before, to the best of our knowledge. The observed objects span from Centaurs up to detached objects (semi-major axis from 10 to more than 100 AU), while in eccentricity they reach values as high as 0.9. The inclinations are mostly below 40°, with one object at about 80° and one in retrograde orbit (2008 YB_3).

At the same time as we acquired our own data, we made an extensive, although not complete, search in the literature of other published V and R magnitudes. We used as our primary reference database the MBOSS 2 article by Hainaut et al. (2012), but we did not take the data directly from their catalog. Instead we took the data from each referenced article to be included in our list. We chose this approach because we need reduced magnitudes (described in Sect. 3.2) to compute the phase curves, which are computed using the heliocentric and geocentric distances at the moment of observation. At the same time, we obtained information regarding the phase angle. Of course we only used data that were reported along with the site and epoch of observation. We obtained the orbital information from JPL-Horizons[9]. For data of rotational light-curves, i.e., many magnitudes reported for the same night, we computed the average value and its standard deviation to use as input. We finally had more than 1800 individual measurements for over a hundred objects. Each individual measurement corresponds to one observing night or entry. We did not reject any data based on their reported error bars.

Before we discuss the results, we stress three important points: (i) we obtained data for 56 objects, but these data alone cannot be used to create phase curves for all the objects, therefore we also consulted the literature. This augmented set of data is called *our database*. (ii) As can be seen in Eq. (1), we cannot split albedo and diameter using H_V alone, therefore whenever we speak about the *brightness* of an object, we refer exclusively to its magnitude and not to its albedo properties or its size, unless explicitly mentioned. (iii) The magnitudes for the phase curves should be averaged over the rotational period to remove the effect of variability that is due to $\Delta m > 0$, which is not the case for individual measurements.

In the following subsections we first describe how we computed the colors for the complete database, and then report how we constructed the phase curves.

[9] http://ssd.jpl.nasa.gov/horizons.cgi

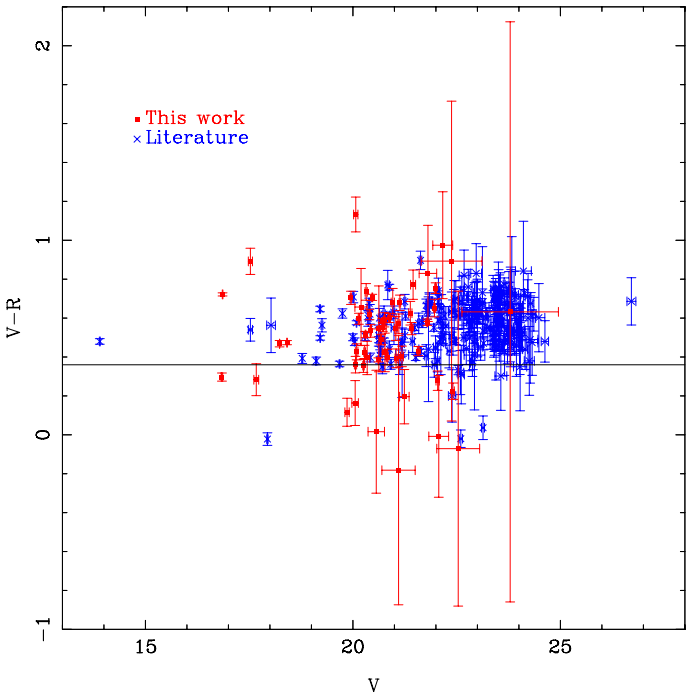

Fig. 1. Color−magnitude diagram for the objects in our database. We show in red the objects that have at least one color measured by us, while objects whose data come from the literature alone are shown in blue. The $(V - R)_\odot$ is shown for reference as a horizontal line.

3.1. Colors

Because it is a compilation from different sources, our database is very heterogeneous. Some objects have many entries, in a few cases more than fifty, while most have fewer than ten entries (72% of the sample). Not all entries have data obtained with both filters; in some cases, only the V filter was used, while in some others only the R filter magnitude is available. Whenever both magnitudes were available for the same night, we computed $(V - R)$. In this way, many objects have more than one measurement of $(V - R)$. In these cases, we computed a weighted average color, which we took as representative for the object. By doing so, we weighted the most precise values of $(V - R)$ instead of considering possible changes of color with phase angle, which is beyond the scope of the present work.

We show the color−magnitude diagram for all objects in our sample in Fig. 1. If at least one entry for a given object was observed by us, we labeled that object "this work", while if all observations for a given object were obtained from the literature, the label "literature" was used. The plot has more than 110 points

because we also show the colors of objects that did not satisfy our criteria for constructing the phase curve (see below).

Most objects shown in the figure are redder than the Sun, $(V-R)_\odot = 0.36$. Nevertheless, there are a few bluer objects, $(V-R) \approx 0$. The great majority of the objects cluster at $V \approx 23$, $(V-R) \approx 0.6$. The figure also clearly shows that our observations have a clear cutoff at about $V = 22.5$, which is due to the size of the telescopes used, with only one object fainter than $V = 23$: 2003 QA_{91}; this has obvious large error bars.

3.2. Phase curves

The main objective of this work is to compute absolute magnitudes, H_V, and phase coefficients, β, of as many objects as possible. These data could be used as complement to the *Herschel* Space Observatory "TNOs are cool" key project. Several papers have already been published presenting H_V of different TNOs (e.g., Sheppard & Jewitt 2002; Rabinowitz et al. 2006, 2007; Perna et al. 2013; Böhnhardt et al. 2014, and others). We do not intend to repeat these works step by step, but to recompute the phase curves and make the most of the increasing amount of data available today. We are aware of the risks that arise as a result of the inhomogeneity of telescopes, instruments, detectors, and epochs. Nevertheless, we consider it important to reanalyze the available data using, if not homogeneous inputs, at least homogeneous techniques.

As mentioned above, we had to deal with the fact that not all entries (i.e., nights of observation for a given object) were complete, in the sense that some objects for a given date were observed only in one filter, V or R. To find a solution for this problem, we decided to construct the individual phase curves using magnitudes measured with the V filter. When V was not available, we used the average color measured above and the R magnitude to obtain V. We decided, for the scope of this work, to not analyze the V and R data separately because we are more interested in obtaining the larger possible quantity of the phase curves. For instance, if we were to use only the V data, without the R data, we would only obtain about 50 phase curves. A similar number of phase curves are obtained when only R data are used, although not necessarily for the same objects.

The next step is to compute the reduced V, whose notation is $V(1,1,\alpha)$, which is the value used in the phase curves. It represents the magnitude of the object if it is located at 1 AU from the Sun and is observed at a distance of 1 AU from Earth.

The reduced magnitude is computed from the values of V and the orbital information as

$$V(1,1,\alpha) = V - 5\log(r\Delta). \quad (4)$$

We are now left with a set $\{V(1,1,\alpha),\alpha\}$ for each object.

For the phase curves we only used data for objects that were observed at least at three different phase angles. We discarded a few objects that had a small coverage in α, which results in unreliable values of H_V. We analyzed a total of 110 objects. For objects with no reported light-curve amplitude we assumed $\Delta m = 0$ and performed a linear regression to measure H_V via

$$V(1,1,\alpha) = H_V + \alpha \times \beta, \quad (5)$$

where β is the change of magnitude per degree, also known as phase coefficient. Each $V(1,1,\alpha)$ was weighted by its error, assumed equal to that of the V magnitude, or propagated from the R magnitude and that of the average color, while α was assumed to have a negligible error. By doing so, we obtained H_V as the y-intercept and β as the slope of Eq. (5).

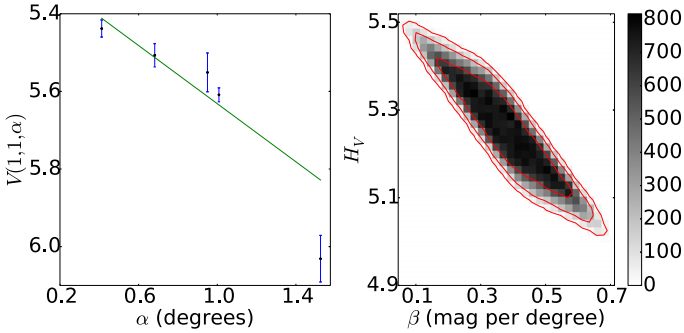

Fig. 2. Example of phase curve of 1996 TL_{66}. *Left*: scatter plot of $V(1,1,\alpha)$ versus α. The line represents the solution for H_V and β as mentioned in the text. *Right*: density plot showing the phase space of solutions of Eq. (5) when $\Delta m \neq 0$, in gray scale. The effect of the Δm may cause values between 5.0 and 5.5 for H_V, while the same is true for $\beta \in (0.041, 0.706)$ mag per degree. The continuous lines (red) show the area that contains 68.3, 95.5, and 99.7% of the solutions.

We used the linear approach instead of using the full H-G system (Bowell et al. 1989) for simplicity because we do not wish to add any more free parameters that will unnecessarily complicate the interpretation of results. We also made use of the results presented in Belskaya & Shevchenko (2000), mentioned in the Introduction, who showed that the opposition effect, the major departure from linearity of the phase curve, is in fact more conspicuous in moderate-albedo objects ($p_V > 0.25$), which is not the case for most of the known TNOs (e.g., Lellouch et al. 2013; Lacerda et al. 2014).

Some objects do have reported rotational light-curves with non-zero Δm (we here use the data reported in Thirouin et al. 2010, 2012). We note that Δm can cover a range of up to half a magnitude in extreme, but rare, cases. Because we used reduced magnitudes obtained on different nights and mostly individual measurements, we modeled the effect of light-curve variations on the value of $V(1,1,\alpha)$. We proceeded as follows: for an object with $\Delta m \neq 0$ we generated from $\{V(1,1,\alpha),\alpha\}$ new sets $\{V_i(1,1,\alpha),\alpha\}$, with i running from 1 to 10 000, where

$$V_i(1,1,\alpha) = V(1,1,\alpha) + rand_i \times \Delta m, \quad (6)$$

$rand_i$ is a random number drawn from a uniform distribution within −1 and 1. By doing so, and feeding these values into Eq. (5), we compiled a set $\{H_{Vi},\beta_i\}$, from where we obtain H_V and β as the average over the 10 000 realizations.

In other words, for objects with $\Delta m > 0$ we have 10 000 different solutions for Eq. (5). We computed the average of the solutions for H_V and β and assumed these values as the most likely result. A graphical representation of the procedure is shown in Fig. 2. The left panel shows the representative phase curve along with the data points and their errors, while the right panel shows a two-dimensional histogram showing the phase-space covered by the 10 000 solutions. This method allowed us to explore the solution space, from which we found some interesting results, such as those unexpected cases with $\beta < 0$, which we discuss in Sect. 5.

All results are shown in Table A.2. The table reports the observed object, H_V and β, the number of points used in the fits, the light-curve amplitude, and the references to the works whose reported magnitudes were used. The phase curves are shown in Figs. A.1–A.110.

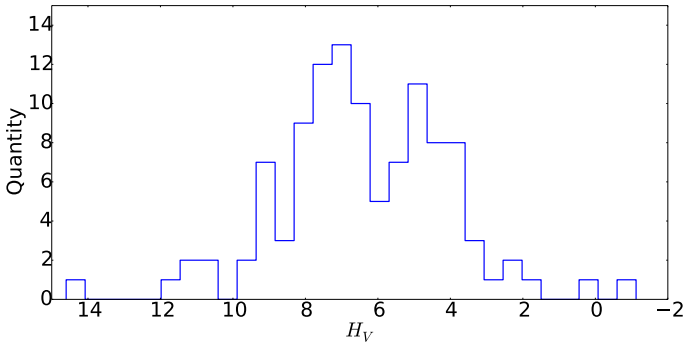

Fig. 3. Histogram showing the H_V distribution.

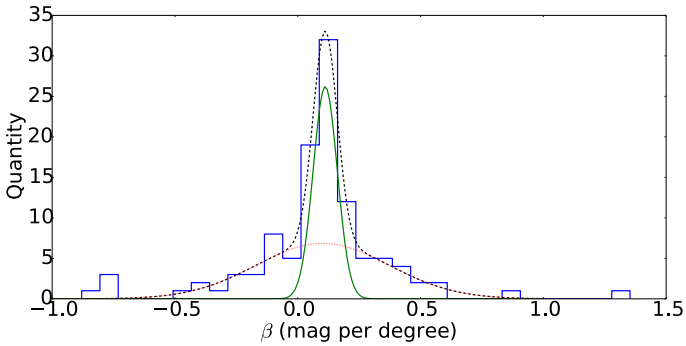

Fig. 4. Histogram showing the β distribution. The dashed black line is the better fit to the distribution, modeled as the sum of two Gaussian distributions (see text). Each individual Gaussian distribution is shown as continuous green and dotted red lines.

4. Results

We measured H_V and β for a total of 110 objects. Figure 3 shows the distribution of H_V resulting from applying our procedure. The distribution looks bimodal, with the larger peak at $H_V \approx 7$ and a second one at $H_V \approx 5$. Our results cover a range from a minimum of $H_V = 14.6$ (2005 UJ_{438}) up to a maximum of -1.12 for Eris. The average value is 6.39, while the median is 6.58. The distribution of β is shown in Fig. 4. The average value is 0.09 mag per degree, while the median is 0.10 mag per degree, with a minimum of -0.88 mag per degree for 2003 GH_{55} and a maximum of 1.35 mag per degree for 2004 GV_9. Almost 60% of the values fall within 0.01 and 0.23 mag per degree.

Curiously, the distribution shown in Fig. 4 seems to be the combination of two different distributions, one wide and shallow, and a second one sharp and tall. To test this possibility, we assumed that the distribution could be fitted by a sum of two Gaussian distributions

$$F(\beta) = C_1 e^{-\frac{(\beta-\beta_1)^2}{2\sigma_1^2}} + C_2 e^{-\frac{(\beta-\beta_2)^2}{2\sigma_2^2}},$$

where C_i, β_i, and σ_i are free parameters.

We ran a minimization script from python (`scipy.optimize.leastsq`) to obtain all six free parameters: $C_1 = 6.8$, $\sigma_1 = 0.27$ mag per degree, $\beta_1 = 0.10$ mag per degree, and $C_2 = 26.2$, $\sigma_2 = 0.05$ mag per degree, $\beta_2 = 0.11$ mag per degree. The best-fitting $F(\beta)$ is shown in Fig. 4, along with the two components. The two-Gaussian model describes the distribution of β very well, both with similar modes but different widths. We return to this model in the Discussion.

Next, we compared our results with those of a few selected works: Rabinowitz et al. (2007), Perna et al. (2013), and Böhnhardt et al. (2014); and then we searched for correlations among our results (H_V, colors, β), orbital elements (semi-major axis, eccentricity, inclination), the absolute magnitudes used in the "TNOs are cool" *Herschel* Space Observatory key project and their measured geometric albedos, and the light-curve amplitude Δm. Orbital elements for each object were obtained from the Lowell Observatory[10].

4.1. Comparison with selected works

On one hand, we selected Rabinowitz et al. (2007, Ra07) because it has the densest phase curves reported for 25 outer solar system objects, while on the other hand, Perna et al. (2013, Pe13) and Böhnhardt et al. (2014, Bo14) presented results in support for the HSO "TNOs are cool" key project. The three works analyze their data following different criteria: Ra07 observed each target on many occasions, even attempting to obtain rotational properties. If a rotational light-curve could be determined, the data were corrected removing the short-term variability, the remaining data were then rebinned in α, and then the phase curves were constructed. Pe13, using less dense data, computed phase curves for a few objects, while average values of β were assumed for objects without enough data . Bo14 only used average values of β.

We report in Table A.3 the comparison between our results and those from Ra07, Pe13, and Bo14. We note that our phase curves include the data reported in these three works.

Overall, the four works agree very well. Nevertheless, some values differ beyond three sigma. For clarity we report these differences here (shown in boldface in Table A.3). With Ra07 Makemake (H_V and β) and Sedna (H_V); with Pe13 2005 UJ_{438} (H_V) and Varda (H_V); with Bo14 2003 GH_{55}, 2004 PG_{115}, and Okyrhoe. In this last case the differences are only in H_V because these authors did not compute the phase curve, but instead used average values of β to obtain absolute magnitudes. Moreover, the errors in our data are somewhat larger than those in Ra07, Pe13, and Bo14. We return to this issue in the discussion.

4.2. Correlations

We searched for possible correlations among pairs of variables. We define here a variable as any given set of quantities representing the population, for instance, the variable β is the set of phase coefficients of the TNOs sample. The correlations were explored using a Spearman test, which has the advantage of being non-parametric because it relies on ordering the data according to rank and running a linear regression through those ranks. The test returned two values. The first one, r_s, gives the level of correlation of the tested variables, $|r_s| \approx 1$ indicates correlated quantities, while $|r_s| \rightarrow 0$ indicates uncorrelated data. The second value is P_{r_s} which indicates the probability of two variables to be uncorrelated, in practical terms, the closer P_{r_s} is to zero, the more likely becomes the result provided by r_s.

One disadvantage of the Spearman test is that it does not consider the errors in the variables. To overcome this problem, we proceeded as follows: we tried to find the correlation among a set $\{x_j, y_j\}$, where each quantity x_j (y_j) has an error of σ_{x_j} (σ_{y_j}), j running from 1 up to N. Then we created 10,000 correlations by creating new sets $\{x_{j_i}, y_{j_i}\}$, where $x_{j_i} = x_j + rand_i \times \sigma_{x_j}$, likewise for y_j. In this case, $rand_i$ is a random number drawn from a normal distribution in $[-1, 1]$. The random number in x_j is not necessarily the same as in y_j.

[10] `ftp://ftp.lowell.edu/pub/elgb/astorb.html`

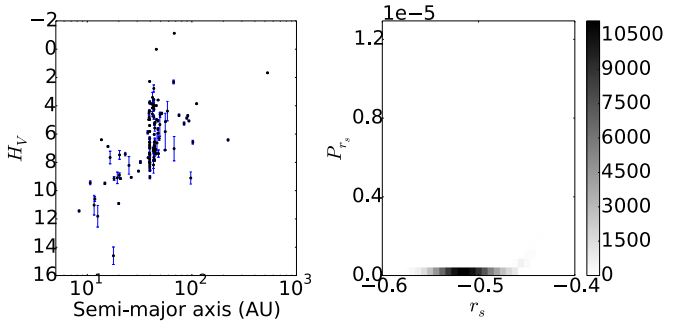

Fig. 5. *Left*: scatter plot of H_V vs. semi-major axis. *Right*: outcome of the 10 000 realizations in form of a two-dimensional histogram in r_s and P_{r_s} which shows the phase space where the solutions lie. In a few cases it is relatively clear that a correlation might exists, while in some other cases large excursions are seen, which indicate that a false correlation could arise in the case of large errors.

Table 1. Correlations.

Variables	r_s	P_{r_s}	Correlation
H_V vs. a	–0.517	7.6×10^{-9}	yes*
H_V(ours) vs. H_V(HSO)	0.987	7.1×10^{-51}	yes
H_V vs. p_V	–0.509	1.8×10^{-5}	yes
β vs. H_V	–0.379	4.5×10^{-5}	weak
H_V vs. Δm	0.359	0.0020	weak
H_V vs. inclination	–0.335	0.0003	weak
H_V vs. e	0.207	0.0299	no*
β vs. Δm	–0.141	0.2358	no
β vs. p_V	0.011	0.9341	no
H_V vs. $V-R$	0.185	0.0532	no
β vs. $V-R$	0.090	0.3474	no
β vs. a	0.233	0.0142	no
β vs. e	0.137	0.1525	no
β vs. inclination	0.140	0.1450	no

Notes. (*) Observational bias.

After performing the 10 000 correlations, we had a set $\{r_{si}, P_{r_si}\}$, which is displayed in the form of density plots to show the likelihood of the correlation to hold against the error bars. All relevant results are displayed in Figs. 5–11. Table 1 shows the result of the correlation tests: the first column shows the variables tested, the second and third column show the nominal values of r_s and P_{r_s} (those where the errors were not accounted for), while the last column reports our interpretation of the density plots of whether the correlation exists or not.

For the scope of the present work we decided not to separate our sample into the subpopulations that appear among Centaurs and TNOs because dividing a sample of 110 objects into smaller samples will only decrease the statistical significance of any possible result. Furthermore, should any real difference arise among any subgroup, this would clearly be seen in any of the tests proposed here, for instance, the fact that no large Centaurs are known, or that the so-called cold classic TNO have low inclinations and tend to be smaller in size than other subpopulations of TNOs. Below we report the most interesting findings of the search for correlations. Thereafter, we discuss some individual cases that showed interesting or anomalous behavior.

H_V vs. semi-major axis: Fig. 5 shows the correlation between absolute magnitude and semi-major axis. This correlation is due to observational bias and accounts for the lack of faint objects detected at large heliocentric distances, while no bright Centaur (we loosely define a Centaur as an object with a semi-major axis below 30 AU) is known to exist.

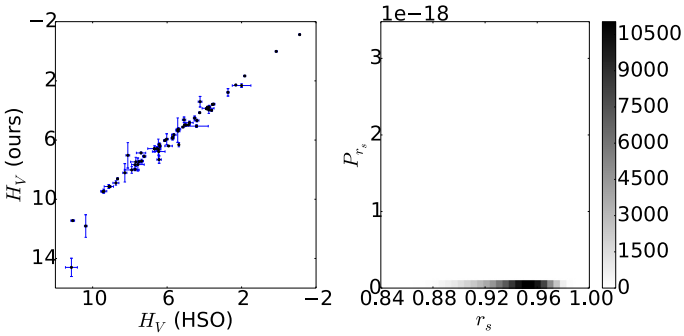

Fig. 6. *Left*: scatter plot of H_V as measured by us vs. (ours). H_V as used within the "TNO's are cool" program (HSO). *Right*: two-dimensional histogram showing the most likely correlations.

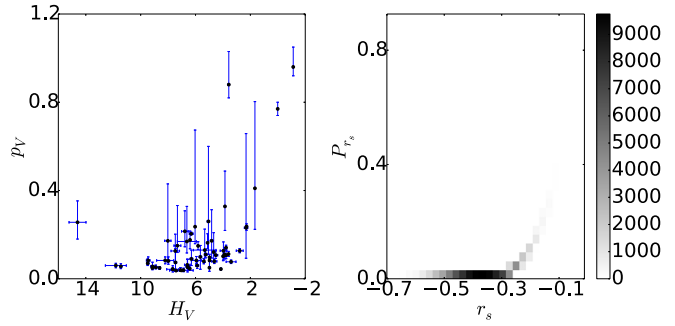

Fig. 7. *Left*: scatter plot of H_V vs. the geometric albedo measured by the "TNOs are cool" program. *Right*: two-dimensional histogram showing the most likely correlations.

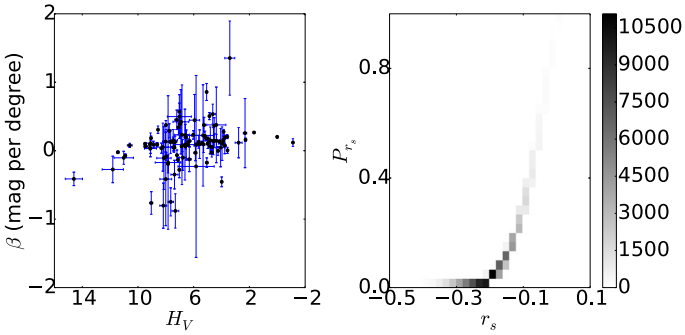

Fig. 8. *Left*: scatter plot of β vs. H_V. *Right*: two-dimensional histogram showing the most likely correlations.

H_V(ours) vs. H_V(HSO): in this case we compared our computed magnitudes with those used by the *Herschel* Space Observatory "TNOs are cool" key project. The correlation is close to 1 (Fig. 6), although it is possible to see a small departure at the faint end with two objects with significantly smaller H_V, they are (250112) 2002 KY_{14} ($H_V = 11.808 \pm 0.763$, Fig. A.50) and (145486) 2005 UJ_{438} ($H_V = 14.602 \pm 0.617$, Fig. A.78). In the first case we revised the data without finding any evident problem and we trust the value to be correct, while in the second case some care should be taken because the minimum value of the phase angle is about 5.8° , leaving most of the phase curve undersampled, which might affect the value of β.

For the sake of comparison, we fitted a linear function to the data according to H_V(ours)= $a + b \times H_V$(HSO), obtaining $b = 1.06 \pm 0.03$ and $a = -0.27 \pm 0.17$. This indicates that

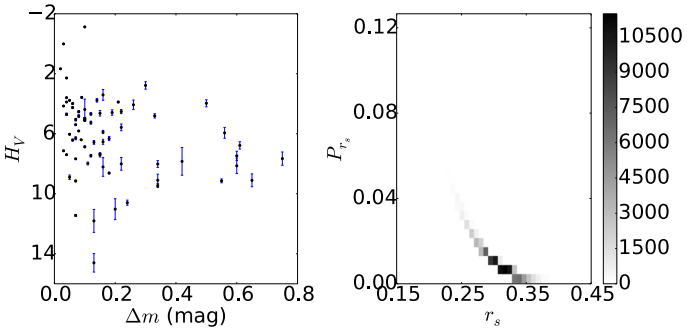

Fig. 9. *Left*: scatter plot of H_V vs. Δm. *Right*: Two-dimensional histogram showing the most likely correlations.

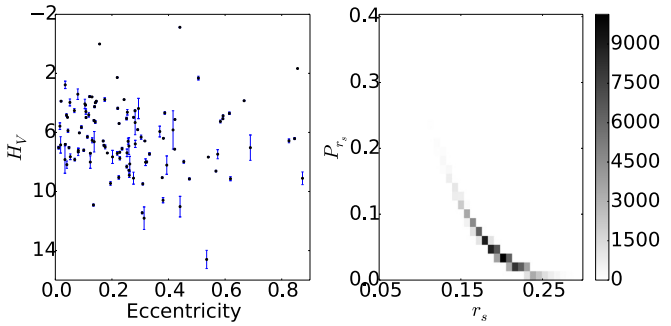

Fig. 10. *Left*: scatter plot of H_V vs. eccentricity. *Right*: two-dimensional histogram showing the most likely correlations.

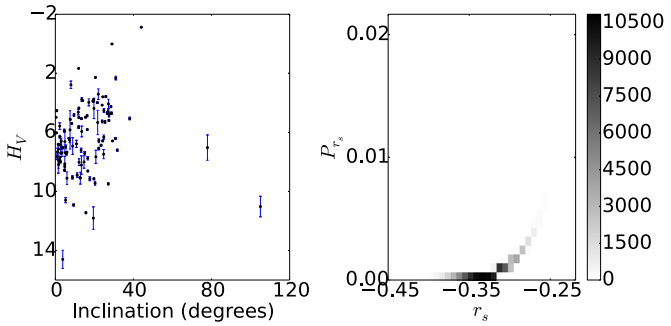

Fig. 11. *Left*: scatter plot of H_V vs. inclination. *Right*: two-dimensional histogram showing the most likely correlations.

although H_V(ours) are very similar to H_V(HSO), they are not identical. This difference between our H_V and those used by the "TNOs are cool" team probably arises because some of theirs were computed using single observations and assuming an average β.

H_V vs. p_V: Fig. 7 shows a correlation between the absolute magnitude and the geometric albedo: the brigher the object, the larger the albedo. This probably reflects the fact that brighter objects tend to be the larger in size as well and are therefore able to retain part of the original volatiles, more reflective species, that smaller objects cannot.

β vs. H_V: H_V seems to have a weak anticorrelation with β, indicating that brighter objects have larger positive slopes than fainter ones. From Fig. 8 one interesting detail arises: there are a few objects with $\beta < 0$ (see also Fig. 4), even considering the error bars and light-curve amplitude (see Table A.2). This issue deserves further study and observations. According to the density map, the weak correlation seems quite consistent within the errors in H_V and β.

H_V vs. Δm: there is a weak correlation between absolute magnitude and Δm, which indicates that brighter objects tend to have lower Δm. Interestingly, among the faint object (fainter than $H_V = 10$) no large (>0.25) amplitudes are found (Fig. 9). We recall that although they are faint objects, they are usually in the range 50 to 100 km[11].

Duffard et al. (2009) presented a similar value for this correlation. Using their results (their Fig. 6), we also see that objects with densities lower than 0.7 g cm^{-3} are unlikely in hydrostatic equilibrium and therefore could have large Δm, which is not reflected in our Fig. 9. These density correspond to ≈400 km (from Fig. S7 in Ortiz et al. 2012), which is roughly $H_V \approx 5.4$. Brighter, possibly larger, objects are in hydrostatic equilibrium and their shapes are better described by Mclaurin spheroids whose Δm are harder to measure because they are symmetric around the minor axis.

H_V vs. eccentricity and inclination: there are two curious cases (Figs. 10 and 11). The first one, H_V vs. eccentricity, indicates that fainter objects tend to have higher eccentricities. This is an observational bias because faint objects are more easily observed close to perihelion, favoring objects with high eccentricties. The second one, H_V vs. inclination, also shows a weak tendency of fainter objects having smaller inclinations. This might be reflecting the known fact that two supopulations are found in the so-called classical trans-Neptunian belt, which are distunguished as a hot and a cold population (from dynamical considerations). The cold, low-inclination population does not have objects as large as the hot, high-inclination, population. Although both tendencies seem significant over the 2-sigma level (>95.5%), only one seems closer to be a correlation with $|r_s| > 0.3$.

Other results: none of the other pairs of variables explored show any significant correlation, therefore their plots are not reported.

Interesting objects: in this paragraph we describe some objects that deserve more discussion.

2060 Chiron: Meech & Belton (1989) detected a coma surrounding Chiron; this result probably influenced the interpretation of latter stellar occultations results (e.g., Bus et al. 1996) that detected secondary events which were associated with jets of material ejected from the surface. A recent reanalysis of all stellar occultation data, along with new photometric data, suggests that Chiron possesses a ring system (Ortiz et al. 2015). These two phenomena, cometary-like activity and the possible ring system, affect the photometric data obtained from Chiron, including the way the photometric measurements are performed, thus increasing the scattering in the phase curve (Fig. A.90).

10199 Chariklo: Braga-Ribas et al. (2014) detected a ring system around Chariklo using data from a stellar occultation. This result helped to interpret long-term changes in photometric and spectroscopic data (Duffard et al. 2014), such as the secular variation in reduced magnitude (Belskaya et al. 2010) and the disappearance of a water-ice absorption feature in its near-infrared spectrum (Guilbert et al. 2009). As for Chiron, the phase curve of Chariklo does not follow a linear trend (Fig. A.89).

[11] See http://public-tnosarecool.lesia.obspm.fr/

Bright objects: those with H_V brighter than 3 have β between 0.11 and 0.27 mag per degree (Figs. A.80, A.94, A.98, A.100, A.103, and A.105). Spectroscopically it is known that these objects (2007 OR_{10}, Eris, Makemake, Orcus, Quaoar, and Sedna) are very different; Eris and Makemake display methane ice absorption features, while Orcus, Quaoar, and 2007 OR_{10} show water ice and probably some hydrocarbons. Therefore, particle size or compaction could play a more important role than composition on the phase curves.

5. Discussion and conclusions

We have observed 56 objects, six of them with no previously reported magnitudes in the literature, to the best of our knowledge. We combined these new V and R magnitudes with an extensive bibliographic survey to compute absolute magnitudes and phase coefficients. In total we report H_V and β for 110 objects. Some of these objects already had reported phase curves, nevertheless, it is important to include new data, always keeping in mind that we combined data from different apparitions for the same object and that surface conditions might have changed between observations.

Regarding the distribution of β, Fig. 4 clearly shows a quasi-symmetric distribution. The maximum and mode coincide to the second decimal place with the average and median values: 0.10 mag per degree. We tested the hypothesis of having a two-population distribution by assuming that each population could be described by a Gaussian function. The fit to the data is quite good, but does this indicate the existence of two *real* subpopulations? One possible explanation regards the quality of the data: There might be a high-quality subsample cluster with a mode of $\beta_2 = 0.11$ mag per degree within a sharp distribution, while the low-quality data are more spread out, but with a very similar mode ($\beta_2 = 0.10$ mag per degree). This would consider as high-quality data those with small errors, precise β, and with (at least) an estimate of Δm. Unfortunately, this is not strictly the case because some of these objects fall within the wings of the wide and shallow distribution. Therefore, even if it is very tempting, we cannot use the sharp distribution as representative of the whole population because we might introduce undesired biases in the results. Moreover, most of the objects fall within the wide distribution, 59%, while 41% fall within the sharp one.

It is clear that there is not one representative value of β for the whole population. Therefore, the use of average values of β to compute H_V should be regarded with caution. The phase coefficients range from −0.88 up to 1.35 mag per degree. On the extreme positive side, the two objects (1996 GQ_{21}, Fig. A.11; and 2004 GV_9, Fig. A.68) have large associated errors. Among the extreme negative values are six objects (1998 KG_{62}, Fig. A.25; 1998 UR_{43}, Fig. A.28; 2002 GP_{32}, Fig. A.47; 2003 GH_{55}, Fig. A.61; 2005 UJ_{438}, Fig. A.78; and Varda, Fig. A.109) with $\beta < 0$, even considering three times the error. Most of these cases are objects whose data are sparse and with few points. Two of them, UJ438 and Varda, have an estimated light-curve amplitude, while the rest has no reported value to the best of our knowledge.

We are not aware of any physical mechanism that could explain a $\beta < 0$ using scattering models. There are some components of the light that could be negative, such as the incoherent second scattering order (Fig. 21 in Shkuratov et al. 2002), which is nonetheless non-dominant, especially for the low values of α that we can observe TNOs with.

These extremes values, either positive or negative, could be due to as yet undetected phenomena, such as poorly determined rotational modulation, ring systems, or cometary-like activity. They deserve more observations.

Some phase curves clearly do not follow a linear trend. Those of Chiron and Chariklo, in fact, do not follow any particular trend at all. It is convenient to bear in mind that the photometric models for understanding the photometric behavior of phase curves were made for objects with nothing else than their bare surface to reflect, scatter, or absorb photons. In the case of these possibly ringed systems the reflected light detected on Earth depends not only on the scattering properties of the material covering Chiron or Chariklo, but also on the particles in the rings and the geometry of the system. With this in mind, we propose that one criterion to seek candidates that bear ring systems is to search for this "non-linear" behavior of the phase curve. As examples, based on the dispersion seen in their phase curves, we propose that 1996 RQ_{20} (Fig. A.12), 1998 SN_{165} (Fig. A.27), or 2004 UX_{10} (Fig. A.71) might be candidates for further studies, among other objects.

The correlations were discussed in their respective paragraphs. Overall, some of them are associated with observational biases (H_V and semi-major axis; H_V and eccentricity), others can be interpreted in terms of known properties of the TNO region (H_V and inclination), while the rest can be considered as weak or non-existing and deserving more data, especially going deeper into the faint end of the population. We do not confirm the proposed anticorrelation between albedo and phase coefficient (see Belskaya et al. 2008 and references therein). One special note about the anticorrelation found between H_V and p_V: it would seem that the correlation is driven principally by the brighter objects. We ran the same test discarding objects brighter than 3 and those associated with the Haumea dynamical group because they form a group that stands apart with particular surface properties, and the relation still holds, $r_s = -0.356$, $P_{r_s} = 0.0092$. Although the correlation does become weaker, without reaching a $3-\sigma$ level, there seems to exists a trend of brighter objects to have larger geometric albedos. An in-depth physical explanation remains yet to be formulated.

Finally, the errors reported in H_V are in some cases larger than in previous works. This reflects the heterogeneity of the sample, how the effect of the rotational variability is considered, and the weighting of the data while performing the linear fits. For instance, we note that all of the objects with $\sigma_{H_V} > 0.1$ mag have either fewer than ten data points or $\Delta m > 0.1$ mag. Taking this into consideration, our results are more accurate than, although not as precise as, previous works and probably more realistic, with the exception of the strategy followed by Rabinowitz et al. (2007).

This work represents the first release of data taken at seven different telescopes in six observatories between late 2011 and mid-2015, which represents a large effort. It is important to mention that more observations are ongoing.

Acknowledgements. Based in part on observations collected at the German-Spanish Astronomical Center, Calar Alto, operated jointly by Max-Planck-Institut für Astronomie and Instituto de Astrofísica de Andalucía (CSIC). Based in part on observations made with the *Isaac Newton* Telescope operated on the island of La Palma by the Isaac Newton Group in the Spanish Observatorio del Roque de los Muchachos of the Instituto de Astrofísica de Canarias. Partially based on data obtained with the 1.5 m telescope, which is operated by the Instituto de Astrofísica de Andalucía at the Sierra Nevada Observatory. Partially based on observations obtained at the Southern Astrophysical Research (SOAR) telescope, which is a joint project of the Ministério da Ciência, Tecnologia, e Inovação (MCTI) da República Federativa do Brasil, the U.S. National Optical Astronomy Observatory (NOAO), the University of North Carolina at Chapel Hill (UNC), and Michigan State University (MSU). Based in part on observations made at the Observatório Astronômico do Sertão de Itaparica operated

by the Observatório Nacional/MCTI, Brazil. Partially based on observations made with the Liverpool Telescope operated on the island of La Palma by Liverpool John Moores University in the Spanish Observatorio del Roque de los Muchachos of the Instituto de Astrofísica de Canarias with financial support from the UK Science and Technology Facilities Council. A.A.C. acknowledges support through diverse grants to FAPERJ and CNPq. J.L.O. acknowledges support from the Spanish Mineco grant AYA-2011-30106-CO2-O1, from FEDER funds and from the Proyecto de Excelencia de la Junta de Andalucía, J.A. 2012-FQM1776. R.D. acknowledges the support of MINECO for his Ramón y Cajal Contract. The authors would like to thank Y. Jiménez-Teja for technical support and P.H. Hasselmann for helpful discussions regarding phase curves. We are grateful to O. Hainaut, whose comments helped us to improve the quality of this manuscript.

References

Barucci, M. A., Romon, J., Doressoundiram, A., et al. 2000, AJ, 120, 496
Barucci, M. A., Böhnhardt, H., Dotto, E., et al. 2002, A&A, 392, 335
Barucci, M. A., Cruikshank, D. P., Dotto, E., et al. 2005, A&A, 439, L1
Barucci, M. A., Alvarez-Candal, A., Merlin, F., et al. 2011, Icarus, 214, 297
Belskaya, I., & Shevchenko, V. 2000, Icarus, 147, 94
Belskaya, I. N., Levasseur-Regourd, A.-C., Shkuratov, Y. G., et al. 2008, in The Solar System Beyond Neptune, eds. M. A. Barucci, H. Boehnhardt, D. P. Cruikshank, et al. (Tucson: Univ. of Arizona Press), 115
Belskaya, I. N., Bagnulo, S., Barucci, M. A., et al. 2010, Icarus, 210, 472
Bonnarel, F., Fernique, P., Bienaymé, O., et al. 2000, A&ASS, 143, 33
Böhnhardt, H., Tozzi, G.-P., Birkle, K., et al. 2001, A&A, 378, 653
Böhnhardt, H., Delsanti, A., Barucci, M. A., et al. 2002, A&A, 395, 297
Böhnhardt, H., Schulz, D., Protopapa, S., & Götz, C. 2014, Earth Moon Planet, 114, 35
Bowell, E., Hapke, B., Domingue, D., et al. 1989, in Asteroids II, eds. R. P. Binzel, T. Gehrels, & M. Shapely Matthews (Tucson: Univ. of Arizona Press), 524
Braga-Ribas, F., Sicardy, B., Ortiz, J. L., et al. 2014, Nature, 508, 72
Brown, W. R., & Luu, J. X. 1997, Icarus, 126, 218
Buie, M. W., & Bus, S. J. 1992, Icarus, 100, 288
Bus, S. J., Buie, M. W., Schleicher, D. G., et al. 1996, Icarus, 123, 478
Carraro, G., Maris, M., Bertin, D., et al. 2006, A&A, 460, L39
Clem, J. L., & Landolt, A. U. 2013, AJ, 146, 88
Davies, J. K., Green, S., McBride, N., et al. 2000, Icarus, 146, 253
Davis, D. R., & Farinella, P. 1997, Icarus, 125, 50
de Bergh, C., Delsanti, A., Tozzi, G. P., et al. 2005, A&A, 437, 1115
Delsanti, A., Böhnhardt, H., Barrera, L, et al. 2001, A&A, 380, 347
DeMeo, F., Fornasier, S., Barucci, M. A., et al. 2009, A&A, 493, 283
Doressoundiram, A., Barucci, M. A., Romon, J., et al. 2001, Icarus, 144, 277
Doressoundiram, A., Peixinho, N., de Bergh, C., et al. 2002, ApJ, 124, 2279
Doressoundiram, A., Peixinho, N., Doucet, C., et al. 2005, Icarus, 174, 90
Dotto, E., Barucci, M. A., Böhnhardt, H., et al. 2003, Icarus, 162, 408
Duffard, R., Lazzaro, D., Pinto, S., et al. 2002, Icarus, 160, 44
Duffard, R., Ortiz, J. L., Thirouin, A., et al. 2009, A&A, 505, 1283
Duffard, R., Pinilla-Alonso, N., Ortiz, J. L., et al. 2014, A&A, 568, A79
Farnham, T. L., & Davies, J. K. 2003, Icarus, 164, 418
Ferrin, I., Rabinowitz, D., Schaefer, B., et al. 2001, ApJ, 548, L243
Fornasier, S., Doressoundiram, A., Tozzi, G. P., et al. 2004, A&A, 421, 353
Fornasier, S., Lazzaro, D., Alvarez-Candal, A., et al. 2014, A&A, 568, L11
Fornasier, S., Hasselmann, P. H., Barucci, M. A., et al. 2015, A&A, 583, A30
Gehrels, T. 1956, ApJ, 123, 331
Gil-Hutton, R., & Licandro, J. 2001, Icarus, 152, 246
Guilbert, A., Barucci, M. A., Brunetto, R., et al. 2009, A&A, 501, 777
Hainaut, O. R., Böhnhardt, H., & Protopapa, S. 2012, A&A, 546, A115
Hapke, B. 1963, JGR, 68, 4571
Jewitt, D. C. 2002, AJ, 123, 1039
Jewitt, D., & Luu, J. 1993, Nature, 362, 730
Jewitt, D., & Luu, J. 1998, AJ, 115, 1667
Jewitt, D., & Luu, J. 2001, AJ, 122, 2099
Jewitt, D. C., & Sheppard, S. S. 2002, AJ, 123, 2110
Lacerda, P., Fornasier, S., Lellouch, E., et al. 2014, ApJ, 793, L2
Lagerkvist, C.-I., Magnusson, P. 1990, A&ASS, 86, 119
Landolt, A. U. 1992, AJ, 104, 340
Lellouch, E., Santos-Sanz, P., Lacerda, P., et al. 2013, A&A, 557, A60
McBride, N., Davies, J. K., Green, S. F., et al. 1999, MNRAS, 306, 799
McBride, N., Green, S. F., Davies, J. K., et al. 2003, Icarus, 161, 501
Meech, K. J., & Belton, M. J. S. 1989, IAU Circ. 4770, 1
Mueller, B. E. A., Tholen, D. J., Hartmann, W. K., et al. 1992, Icarus, 97, 150
Müller, T. G., Lellouch, E., Böhnhardt, H., et al. 2007, Earth Moon Planets, 105, 209
Müller, T. G., Lellouch, E., Stansberry, J., et al. 2010, A&A, 518, A146
Nelson, R. M., Hapke, B. W., Smythe, W. D., et al. 2000, Icarus, 147, 545
Ortiz, J. L., Sota, A., Moreno, R., et al. 2004, A&A, 420, 383
Ortiz, J. L., Sicardy, B., Braga-Ribas, F., et al. 2012, Nature, 491, 566
Ortiz, J. L., Duffard, R., Pinilla-Alonso, N., et al. 2015, A&A, 576, A18
Peixinho, N., Lacerda, P., Ortiz, J. L., et al. 2001, A&A, 371, 753
Peixinho, N., Böhnhardt, H., Belskaya, I., et al. 2004, Icarus, 170, 153
Peixinho, N., Delsanti, A., Guilbert-Lepoutre, A., et al. 2012, A&A, 546, A86
Perna, D., Barucci, M. A., Fornasier, S., et al. 2010, A&A, 510, A53
Perna, D., Dotto, E., Barucci, M. A., et al. 2013, A&A, 555, A49
Pinilla-Alonso, N., Alvarez-Candal, A., Melita, M., et al. 2013, A&A 550, A13
Rabinowitz, D. K., Barkume, K., Brown, M. E., et al. 2006, ApJ, 639, 1238
Rabinowitz, D. L., Schaffer, B. E., & Tourtellotte, W. 2007, AJ, 133, 26
Romanishin, W., & Tegler, S. C. 1999, Nature, 398, 129
Romanishin, W., Tegler, S. C., Levine, J., et al. 1997, AJ, 113, 1893
Romanishin, W., Tegler, S. C., Consolmagno, G. J. 2010, AJ, 140, 29
Romon-Martin, J., Barucci, M. A., de Bergh, C., et al. 2002, Icarus, 160, 59
Santos-Sanz, P., Ortiz, J. L., Barrera, L., et al. 2009, A&A, 494, 693
Schaefer, B. E., & Rabinowitz, D. L. 2002, Icarus, 160, 52
Schaller, E., & Brown, M. 2007, ApJ, 659, L61
Sheppard, S. S. 2010, AJ, 139, 1394
Sheppard, S. S., & Jewitt, D. C. 2002, AJ, 124, 1757
Shkuratov, Y., Ovcharenko, A., Zubko, E., et al. 2002, Icarus, 159, 396
Snodgrass, C., Carry, B., Dumas, C., et al. 2010, A&A, 511, A72
Stetson, P. B. 1990, PASP, 102, 932
Tegler, S. C., & Romanishin, W. 1997, Icarus, 126, 212
Tegler, S. C., & Romanishin, W. 2000, Nature, 407, 979
Tegler, S. C., & Romanishin, W. 2003, Icarus, 161, 181
Tegler, S. C., Romanishin, W., Stone, A., et al. 1997, AJ, 114, 1230
Tegler, S. C., Romanishin, W., & Consolmagno, G. J. 2003, ApJ, 599, L49
Thirouin, A., Ortiz, J. L., Duffard, R., et al. 2010, A&A, 522, A93
Thirouin, A., Ortiz, J. L., Campo-Bagatin A., et al. 2012, MNRAS, 424, 3156
Vereš, P., Jedicke, R., Fitzsimmons, A., et al. 2015, Icarus, 261, 34

Appendix A: Additional tables and figures

Table A.1. Observations.

Object	V	R	Night	r (AU)	Δ (AU)	α (degress)	Telescope	Notes
24835 1995 SM_{55}	19.898 ± 0.216	19.170 ± 0.132	2012-12-09	38.4165	37.6015	0.8285	CAHA2.2	(1)
26181 1996 GQ_{21}	21.536 ± 0.192	20.900 ± 0.155	2014-05-29	42.6600	41.6917	0.4020	SOAR	(1)
26181 1996 GQ_{21}	21.760 ± 0.217	20.516 ± 0.086	2013-06-10	42.3455	41.4599	0.6737	INT	
26181 1996 GQ_{21}	21.775 ± 0.233		2013-06-11	42.3464	41.4692	0.6939	INT	(1)
40314 1999 KR_{16}	21.871 ± 0.132	20.767 ± 0.083	2013-06-03	35.3552	34.4522	0.7536	CAHA3.5	
40314 1999 KR_{16}	21.586 ± 0.091	20.905 ± 0.085	2014-04-02	35.2260	34.4426	1.0274	SOAR	(1)
47171 1999 TC_{36}	20.373 ± 0.134	19.504 ± 0.087	2013-09-03	30.5720	29.8969	1.4249	OSN	(1)
47932 2000 GN_{171}	21.313 ± 0.070	20.852 ± 0.069	2014-04-02	28.4086	27.6404	1.3140	SOAR	(1)
82075 2000 YW_{134}	21.219 ± 0.401	21.039 ± 0.407	2012-12-09	44.6975	44.1306	1.0432	CAHA2.2	(1)
82158 2001 FP_{185}	21.407 ± 0.489	20.779 ± 0.297	2013-04-14	35.4526	34.4818	0.4155	OSN	
82158 2001 FP_{185}	22.354 ± 0.631	20.723 ± 0.399	2013-05-11	35.4714	34.5972	0.8229	CAHA3.5	(1)
2001 KD_{77}	21.799 ± 0.181	21.121 ± 0.110	2013-06-03	35.9812	35.0132	0.4968	CAHA3.5	
139775 2001 QG_{298}	22.068 ± 0.239	22.076 ± 0.202	2013-07-17	31.7844	31.6575	1.8231	CAHA3.5	(1)
55565 2002 AW_{197}	20.720 ± 0.233	19.849 ± 0.116	2013-04-15	46.0579	45.5946	1.1096	OSN	
55565 2002 AW_{197}		19.900 ± 0.173	2013-04-17	46.0589	45.6247	1.1283	OSN	(1,2)
2002 GH_{32}	21.988 ± 0.203	21.726 ± 0.303	2013-06-11	43.4742	42.6321	0.7500	INT	(1)
2002 GP_{32}	22.124 ± 0.087	21.788 ± 0.069	2013-06-11	32.3989	31.4001	0.3222	INT	(1)
2002 GP_{32}	21.824 ± 0.631	22.023 ± 0.037	2013-07-16	32.4100	31.6764	1.2527	CAHA3.5	
95626 2002 GZ_{32}	20.133 ± 0.201	19.829 ± 0.157	2013-04-14	18.5160	17.6439	1.5778	OSN	
119951 2002 KX_{14}		20.375 ± 0.253	2013-06-10	39.2847	38.2818	0.2282	INT	
250112 2002 KY_{14}	19.943 ± 0.136	19.383 ± 0.090	2012-12-08	9.5689	8.8098	3.9111	CAHA2.2	
250112 2002 KY_{14}	20.413 ± 0.091	19.550 ± 0.100	2012-12-11	9.5725	8.8448	4.1247	CAHA2.2	
307261 2002 MS_4	20.064 ± 0.053	18.907 ± 0.073	2013-06-03	47.0005	46.0946	0.5670	CAHA3.5	(3)
307261 2002 MS_4	20.184 ± 0.270	20.406 ± 0.616	2013-05-10	47.0046	46.3190	0.9151	CAHA3.5	(3)
55637 2002 UX_{25}	19.474 ± 0.106	19.632 ± 0.116	2011-10-31	41.4407	40.4513	0.1105	CAHA2.2	(1)
55637 2002 UX_{25}	20.203 ± 0.072	19.606 ± 0.044	2012-10-16	41.3080	40.3379	0.3268	CAHA2.2	
55637 2002 UX_{25}	20.286 ± 0.084	20.164 ± 0.097	2012-12-11	41.2868	40.5805	0.9553	CAHA2.2	
55637 2002 UX_{25}	19.800 ± 0.085	19.545 ± 0.077	2013-09-02	41.1853	40.6445	1.1965	OSN	(1)
55638 2002 VE_{95}	20.490 ± 0.104	19.713 ± 0.106	2012-12-11	28.8622	27.9090	0.4964	CAHA2.2	
55638 2002 VE_{95}	21.223 ± 0.416	20.003 ± 0.171	2011-10-31	28.6992	27.9126	1.2313	CAHA2.2	(1)
119979 2002 WC_{19}	21.099 ± 0.402	21.281 ± 0.563	2012-12-09	41.7521	40.7709	0.1179	CAHA2.2	(1,3)
127546 2002 XU_{93}	21.716 ± 0.401	21.131 ± 0.294	2012-12-11	21.5317	20.9261	2.0983	CAHA2.2	
127546 2002 XU_{93}	21.565 ± 0.334	21.868 ± 0.535	2012-12-10	21.5310	20.9301	2.1084	CAHA2.2	(1)
127546 2002 XU_{93}	21.214 ± 0.260	21.033 ± 0.213	2012-12-08	21.5296	20.9391	2.1302	CAHA2.2	
127546 2002 XU_{93}	21.007 ± 0.144	21.180 ± 0.162	2012-10-16	21.4937	21.3872	2.6493	CAHA2.2	
120132 2003 FY_{128}	20.034 ± 0.386	19.541 ± 0.299	2013-04-15	39.1861	38.1980	0.2555	OSN	
120132 2003 FY_{128}	21.063 ± 0.200	20.254 ± 0.186	2013-04-16	39.1865	38.2004	0.2731	OSN	
120178 2003 OP_{32}	20.269 ± 0.124	19.794 ± 0.166	2012-09-16	41.7560	40.8552	0.6137	CAHA2.2	
120178 2003 OP_{32}	20.084 ± 0.139	20.248 ± 0.185	2012-09-17	41.7562	40.8621	0.6310	CAHA2.2	(1)
120178 2003 OP_{32}	20.168 ± 0.100	19.950 ± 0.082	2011-09-24	41.6606	40.8276	0.7714	CAHA2.2	
120178 2003 OP_{32}	20.044 ± 0.155	19.891 ± 0.215	2011-09-25	41.6609	40.8367	0.7886	CAHA2.2	
120178 2003 OP_{32}	20.828 ± 0.226	20.894 ± 0.283	2012-10-17	41.7642	41.1806	1.1117	CAHA2.2	(1)
120178 2003 OP_{32}		19.686 ± 0.127	2011-10-31	41.6705	41.2996	1.2691	CAHA2.2	(1)
2003 QA_{91}	23.790 ± 1.163	23.158 ± 0.933	2013-06-11	44.6206	44.3877	1.2746	INT	(1,3)
120181 2003 UR_{292}	22.377 ± 0.734	21.484 ± 0.370	2012-09-19	26.7683	25.9857	1.3730	CAHA2.2	
143707 2003 UY_{117}	22.665 ± 1.201	20.853 ± 0.266	2011-10-31	32.8608	31.8758	0.2149	CAHA2.2	(1)
143707 2003 UY_{117}	20.503 ± 0.201	20.614 ± 0.258	2011-09-25	32.8502	32.0036	0.9558	CAHA2.2	
143707 2003 UY_{117}		21.754 ± 0.405	2012-09-17	32.9610	32.2100	1.1793	CAHA2.2	(1)
84922 2003 VS_2	19.914 ± 0.219	19.129 ± 0.128	2012-12-09	36.5176	35.5619	0.3745	CAHA2.2	(1)
84922 2003 VS_2	20.429 ± 0.200	19.973 ± 0.247	2012-10-17	36.5148	35.8418	1.1682	CAHA2.2	(1)
136204 2003 WL_7	21.377 ± 0.437	20.018 ± 0.155	2011-10-31	14.9614	14.2362	2.6674	CAHA2.2	(1)
136204 2003 WL_7	20.930 ± 0.142	20.672 ± 0.087	2012-10-15	15.0067	14.5833	3.5000	CAHA2.2	
120216 2004 EW_{95}	21.131 ± 0.181	20.513 ± 0.144	2014-05-29	27.0955	26.2375	1.1547	SOAR	(1)
90568 2004 GV_9	20.362 ± 0.029	20.053 ± 0.038	2014-04-02	39.3485	38.5014	0.7870	SOAR	(1)
307982 2004 PG_{115}		20.183 ± 0.247	2013-09-03	37.3300	36.3912	0.5687	OSN	(1)
307982 2004 PG_{115}	21.321 ± 0.212	20.414 ± 0.097	2013-07-18	37.3077	36.4746	0.9090	CAHA3.5	
2004 PT_{107}	22.791 ± 0.442	21.689 ± 0.183	2012-10-16	38.2606	37.7248	1.2636	CAHA2.2	
2004 PT_{107}	21.906 ± 0.284	20.994 ± 0.179	2013-06-11	38.2517	37.8609	1.4142	INT	(1)
144897 2004 UX_{10}	19.474 ± 0.106	19.632 ± 0.116	2011-10-31	39.0037	38.0264	0.2566	CAHA2.2	(1)
144897 2004 UX_{10}	20.534 ± 0.083	19.905 ± 0.052	2012-10-16	39.0466	38.0789	0.3597	CAHA2.2	
144897 2004 UX_{10}	19.517 ± 0.150	19.840 ± 0.216	2011-09-25	38.9996	38.1471	0.7902	CAHA2.2	
144897 2004 UX_{10}	20.245 ± 0.104	19.833 ± 0.070	2011-09-24	38.9994	38.1563	0.8129	CAHA2.2	
144897 2004 UX_{10}	20.576 ± 0.195	20.110 ± 0.107	2012-09-19	39.0436	38.2544	0.9261	CAHA2.2	

Notes. (1) Average ext. coeff. (2) Average zero points. (3) Never reported before.

Table A.1. continued.

Object	V	R	Night	r (AU)	Δ (AU)	α (degress)	Telescope	Notes
230965 2004 XA_{192}	20.508 ± 0.101	20.047 ± 0.100	2012-12-11	35.6167	34.8167	0.9358	CAHA2.2	(3)
230965 2004 XA_{192}	20.110 ± 0.144	19.718 ± 0.089	2012-12-10	35.6169	34.8209	0.9453	CAHA2.2	(1,3)
230965 2004 XA_{192}	20.249 ± 0.184	21.061 ± 0.211	2012-12-08	35.6187	34.8313	0.9649	CAHA2.2	(3)
230965 2004 XA_{192}	20.468 ± 0.218	19.638 ± 0.109	2011-10-31	35.6725	35.2058	1.4196	CAHA2.2	(1,3)
230965 2004 XA_{192}	20.278 ± 0.122	19.658 ± 0.176	2012-09-16	35.6294	35.8013	1.5890	CAHA2.2	(3)
303775 2005 QU_{182}	21.078 ± 0.123	20.522 ± 0.088	2013-07-18	50.1479	49.9291	1.1384	CAHA3.5	
145451 2005 RM_{43}	20.033 ± 0.165	19.691 ± 0.127	2011-10-31	35.5824	34.6917	0.7200	CAHA2.2	(1)
145451 2005 RM_{43}	19.981 ± 0.123	19.808 ± 0.063	2012-10-15	35.7194	34.9774	1.0843	CAHA2.2	
145451 2005 RM_{43}	19.832 ± 0.156	19.347 ± 0.206	2011-09-25	35.5692	35.0655	1.4107	CAHA2.2	
145451 2005 RM_{43}	19.799 ± 0.066	19.816 ± 0.073	2011-09-24	35.5688	35.0795	1.4241	CAHA2.2	
145452 2005 RN_{43}	20.116 ± 0.149	19.287 ± 0.104	2013-09-02	40.6506	39.6582	0.2571	OSN	(1)
145452 2005 RN_{43}	19.940 ± 0.117	19.398 ± 0.172	2012-09-16	40.6611	39.7232	0.5098	CAHA2.2	
145452 2005 RN_{43}	20.100 ± 0.235	19.414 ± 0.109	2012-09-19	40.6610	39.7405	0.5668	CAHA2.2	
145452 2005 RN_{43}	20.016 ± 0.090	19.453 ± 0.057	2011-09-24	40.6726	39.7937	0.6834	CAHA2.2	
145452 2005 RN_{43}	20.099 ± 0.174	19.526 ± 0.092	2011-10-31	40.6714	40.2388	1.2623	CAHA2.2	(1)
145453 2005 RR_{43}	20.118 ± 0.094	19.925 ± 0.109	2012-12-11	39.0136	38.1198	0.6082	CAHA2.2	
145453 2005 RR_{43}	20.365 ± 0.220	19.547 ± 0.101	2011-10-31	38.8984	37.9956	0.6200	CAHA2.2	(1)
145453 2005 RR_{43}	20.067 ± 0.075	19.828 ± 0.071	2011-09-24	38.8883	38.3445	1.2540	CAHA2.2	
145480 2005 TB_{190}	21.305 ± 0.050	20.700 ± 0.049	2013-09-03	46.2370	45.2423	0.2139	OSN	(1)
145480 2005 TB_{190}	21.622 ± 0.334	20.641 ± 0.112	2013-07-17	46.2395	45.6431	1.0304	CAHA3.5	(1)
145480 2005 TB_{190}	22.596 ± 0.648	21.191 ± 0.290	2012-09-17	46.2640	45.2744	1.1793	CAHA2.2	(1)
145480 2005 TB_{190}	21.486 ± 0.364	20.436 ± 0.194	2012-12-08	46.2569	46.2518	1.2193	CAHA2.2	
145486 2005 UJ_{438}	20.981 ± 0.470	20.918 ± 0.460	2013-05-05	9.3817	9.0079	5.8384	OSN	
145486 2005 UJ_{438}	21.517 ± 1.266	20.113 ± 0.367	2013-05-08	9.3875	9.0602	5.9318	OSN	(1)
145486 2005 UJ_{438}	20.675 ± 0.209	19.703 ± 0.140	2012-12-08	9.1080	8.9316	6.1615	CAHA2.2	
202421 2005 UQ_{513}	21.388 ± 0.342	20.421 ± 0.217	2013-09-02	48.4570	47.7451	0.8554	OSN	(1)
202421 2005 UQ_{513}	20.347 ± 0.206	19.981 ± 0.164	2012-12-09	48.5130	48.0673	1.0390	CAHA2.2	(1)
2007 OC_{10}	20.994 ± 0.185	20.435 ± 0.094	2013-07-17	35.6259	34.7611	0.8738	CAHA3.5	(1)
225088 2007 OR_{10}	21.358 ± 0.476	20.904 ± 0.665	2013-09-03	86.8923	85.8991	0.1105	OSN	(1)
225088 2007 OR_{10}	22.061 ± 0.653	21.515 ± 0.449	2012-09-17	86.6596	85.7407	0.2647	CAHA2.2	(1)
225088 2007 OR_{10}	21.700 ± 0.158		2015-07-20	87.3397	86.5163	0.3975	Live	(1)
225088 2007 OR_{10}	21.974 ± 0.166		2015-07-19	87.3391	86.5260	0.4068	Live	(1)
225088 2007 OR_{10}	21.897 ± 0.253	20.991 ± 0.106	2013-07-17	86.8608	86.0473	0.4086	CAHA3.5	(1)
225088 2007 OR_{10}	21.727 ± 0.142		2015-07-17	87.3381	86.5405	0.4199	Live	(1)
309239 2007 RW_{10}	21.240 ± 0.115	21.044 ± 0.079	2013-07-17	28.3441	28.2058	2.0419	CAHA3.5	(1)
342842 2008 YB_3	18.988 ± 0.065	18.359 ± 0.063	2013-04-16	7.3259	7.5578	7.5275	OSN	
2013 AZ_{60}	19.987 ± 0.096	19.827 ± 0.111	2013-04-15	8.6654	8.7576	6.5739	OSN	(3)
2013 AZ_{60}	20.188 ± 0.136	20.019 ± 0.127	2013-04-14	8.6676	8.7455	6.5840	OSN	(3)
65489 Ceto	22.003 ± 0.558	21.753 ± 0.731	2013-05-11	34.1466	33.1959	0.5792	CAHA3.5	(1)
65489 Ceto	21.684 ± 0.657	21.928 ± 0.882	2013-07-21	34.3227	34.0991	1.6579	CAHA3.5	(1)
10199 Chariklo	18.812 ± 0.183	18.321 ± 0.158	2014-05-29	14.8053	13.8611	1.4804	SOAR	(1)
10199 Chariklo		18.379 ± 0.035	2014-05-22	14.8000	13.8959	1.8265	OASI	(1)
2060 Chiron	18.505 ± 0.056	18.349 ± 0.037	2012-10-16	17.3090	16.6359	2.4772	CAHA2.2	
2060 Chiron	18.263 ± 0.132	17.843 ± 0.080	2012-12-08	17.3610	17.5362	3.1833	CAHA2.2	
136108 Haumea	17.429 ± 0.107	17.161 ± 0.108	2013-05-06	50.8365	50.0445	0.7069	OSN	(1,2)
136108 Haumea	17.580 ± 0.078	17.250 ± 0.073	2013-05-08	50.8362	50.0582	0.7273	OSN	(1)
136472 Makemake	16.966 ± 0.104	16.421 ± 0.105	2013-05-06	52.3120	51.7204	0.8969	OSN	(1,2)
136472 Makemake		16.469 ± 0.091	2013-05-07	52.3122	51.7330	0.9070	OSN	(1)
136472 Makemake	17.241 ± 0.070	16.796 ± 0.060	2013-05-08	52.3123	51.7449	0.9162	OSN	(1)
5145 Pholus	21.677 ± 0.075	20.911 ± 0.035	2013-06-10	25.2536	24.2802	0.6679	INT	
5145 Pholus	21.765 ± 0.181	21.221 ± 0.190	2013-06-11	25.2552	24.2817	0.6685	INT	(1)
120347 Salacia	20.482 ± 0.121	20.212 ± 0.086	2011-09-24	44.2535	43.3414	0.5446	CAHA2.2	
120347 Salacia	20.558 ± 0.231	20.713 ± 0.326	2011-09-25	44.2537	43.3440	0.5505	CAHA2.2	
120347 Salacia	20.800 ± 0.146	20.309 ± 0.076	2012-10-15	44.3415	43.5369	0.7637	CAHA2.2	
120347 Salacia	20.795 ± 0.267	20.128 ± 0.146	2011-10-31	44.2619	43.6166	0.9799	CAHA2.2	(1)
88611 Teharonhiawako	22.538 ± 0.517	22.609 ± 0.623	2012-09-16	45.1115	44.1527	0.3812	CAHA2.2	(3)
42355 Typhon	20.504 ± 0.358	19.920 ± 0.365	2013-05-11	19.0989	18.3380	2.0288	CAHA3.5	(1)
174567 Varda	20.387 ± 0.057	19.722 ± 0.060	2013-06-03	47.3363	46.3863	0.4357	CAHA3.5	
174567 Varda	20.517 ± 0.290	19.948 ± 0.616	2013-05-10	47.3444	46.4795	0.6414	CAHA3.5	
174567 Varda	20.474 ± 0.150	20.235 ± 0.132	2013-05-05	47.3456	46.5173	0.7075	OSN	
174567 Varda	20.116 ± 0.084	19.918 ± 0.089	2013-04-14	47.3528	46.7400	0.9715	OSN	

Table A.2. Absolute magnitudes.

Object	H_V	β (mag per degree)	N	Δm	References
15760 1992 QB_1	7.839 ± 0.097	−0.193 ± 0.132	3	–	TR00,JL01,Bo01
15788 1993 SB	7.995 ± 0.059	0.374 ± 0.066	5	–	Da00,TR00,GH01,JL01,De01
15789 1993 SC	7.393 ± 0.020	0.050 ± 0.017	8	0.04	JL98,Da00,Te97,JL01,TR97
1994 EV_3	8.183 ± 0.247	−0.803 ± 0.329	3	–	Bo02,Bo01,GH01
16684 1994 JQ_1	7.031 ± 0.078	0.570 ± 0.125	5	–	Bo02,TR03,GH01
15820 1994 TB	8.017 ± 0.226	0.133 ± 0.152	9	0.34	Da00,RT99,De01,JL01,TR97
19255 1994 VK_8	7.840 ± 0.923	−0.173 ± 0.976	3	0.42	TR00,Do01,RT99
1995 HM_5	8.315 ± 0.100	0.037 ± 0.074	5	–	RT99,GH01,Ba00
32929 1995 QY_9	8.136 ± 0.515	−0.108 ± 0.459	4	0.60	Da00,RT99,GH01
24835 1995 SM_{55}	4.584 ± 0.178	0.139 ± 0.198	8	0.19	TR03,MB03,GH01,De01,Bo01,Do02,**TW**
26181 1996 GQ_{21}	5.073 ± 0.050	0.858 ± 0.124	6	0.10	MB03,Bo02,**TW**
1996 RQ_{20}	7.201 ± 0.073	−0.065 ± 0.075	5	–	RT99,De01,JL01,Sn10,Bo01
1996 RR_{20}	6.986 ± 0.128	0.391 ± 0.210	3	–	Bo02,TR00,JL01
19299 1996 SZ_4	8.564 ± 0.034	0.307 ± 0.054	4	–	TR00,Da00,JL01,Bo02
1996 TK_{66}	7.031 ± 0.086	−0.280 ± 0.115	3	–	TR00,JL01,Do02
15874 1996 TL_{66}	5.257 ± 0.100	0.375 ± 0.112	5	0.12	JL01,RT99,JL98,Da00,Bo01
19308 1996 TO_{66}	4.806 ± 0.144	0.150 ± 0.197	7	0.33	JL98,Da00,RT99,GH01,Sh10,JL01,Bo01
15875 1996 TP_{66}	7.461 ± 0.084	0.127 ± 0.072	5	0.12	RT99,JL01,JL98,Da00,Bo01
118228 1996 TQ_{66}	8.006 ± 0.422	−0.415 ± 0.680	4	0.22	RT99,JL01,GH01,Da00
1996 TS_{66}	6.535 ± 0.167	0.083 ± 0.220	4	0.16	JL01,RT99,JL98,Da00
33001 1997 CU_{29}	6.808 ± 0.057	0.075 ± 0.087	4	–	Do01,TR00,Ba00,JL01
1997 QH_4	7.216 ± 0.143	0.451 ± 0.142	4	–	TR00,JL01,Bo02,De01
24952 1997 QJ_4	7.754 ± 0.113	0.290 ± 0.103	5	–	De01,GH01,Da00,JL01,Bo02
91133 1998 HK_{151}	7.340 ± 0.056	0.127 ± 0.088	5	0.15	Bo01,Do01,MB03,Do02
385194 1998 KG_{62}	7.647 ± 0.194	−0.748 ± 0.205	3	–	Bo02,GH01,Do01
26308 1998 SM_{165}	5.938 ± 0.363	0.446 ± 0.376	3	0.56	MB03,TR00,De01
35671 1998 SN_{165}	5.879 ± 0.109	−0.031 ± 0.115	6	0.16	De01,MB03,Do01,Fo04,GH01,JL01
1998 UR_{43}	9.047 ± 0.108	−0.764 ± 0.165	3	–	GH01,De01
33340 1998 VG_{44}	6.599 ± 0.205	0.228 ± 0.158	3	0.10	Do02,Bo01,Do01
1999 CD_{158}	5.289 ± 0.092	0.092 ± 0.119	3	–	Do02,Sn10,De01
26375 1999 DE_9	5.120 ± 0.024	0.183 ± 0.032	36	0.10	Ra07,DM09,MB03,Te03,Do02,JL01,De01
1999 HS_{11}	6.843 ± 0.555	0.233 ± 0.728	3	–	Px04,TR03,Do01
40314 1999 KR_{16}	6.316 ± 0.139	−0.126 ± 0.180	4	0.18	Bo02,JL01,**TW**
44594 1999 OX_3	7.980 ± 0.092	−0.086 ± 0.057	12	0.11	Do01,Do02,De01,Pe10,TR00,Bo14,Do05,MB03,Px04,Sh10
86047 1999 OY_3	6.579 ± 0.044	0.067 ± 0.042	4	–	Do02,TR00,Sn10,Bo02
86177 1999 RY_{215}	7.097 ± 0.084	0.341 ± 0.111	3	–	Sn10,Bo02,Do01
47171 1999 TC_{36}	5.395 ± 0.030	0.111 ± 0.027	45	0.07	Ra07,Te03,MB03,De01,Do03,DM09,Do01,Bo01,**TW**
29981 1999 TD_{10}	9.105 ± 0.430	0.033 ± 0.122	21	0.65	MB03,Ra07,De01,TR03,Do02
47932 2000 GN_{171}	6.776 ± 0.243	−0.101 ± 0.186	29	0.61	Ra07,MB03,Bo02,DM09,**TW**
138537 2000 OK_{67}	6.629 ± 0.694	0.089 ± 0.518	3	–	Do02,De01
82075 2000 YW_{134}	4.378 ± 0.687	0.377 ± 0.552	3	0.10	SS09,Do05,**TW**
82158 2001 FP_{185}	6.420 ± 0.062	0.123 ± 0.052	5	0.06	Te03,Px04,Do05,**TW**
2001 KA_{77}	5.646 ± 0.090	0.130 ± 0.095	3	–	Do05,Px04,Do02
2001 KD_{77}	6.299 ± 0.099	0.141 ± 0.082	3	0.07	Px04,Do02,**TW**
42301 2001 UR_{163}	4.529 ± 0.063	0.364 ± 0.117	3	0.08	Do05,SS09,Pe10
55565 2002 AW_{197}	3.593 ± 0.023	0.206 ± 0.029	39	0.04	Ra07,DM09,Fo04,**TW**
2002 GP_{32}	7.133 ± 0.027	−0.135 ± 0.036	4	0.03	Do05,**TW**
95626 2002 GZ_{32}	7.419 ± 0.126	0.043 ± 0.064	29	0.15	Ra07,Fo04,Do05,Te03,**TW**
119951 2002 KX_{14}	4.978 ± 0.017	0.114 ± 0.031	20	–	Ra07,Ro10,Bo14,DM09,**TW**
250112 2002 KY_{14}	11.808 ± 0.763	−0.274 ± 0.193	4	0.13	Bo14,Pe10,**TW**
73480 2002 PN_{34}	8.618 ± 0.054	0.090 ± 0.027	57	0.18	Ra07,Pe10,Te03

Notes. BB92 = Buie & Bus (1992), Mu92 = Mueller et al. (1992), BL97 = Brown & Luu (1997), TR97 = Tegler & Romanishin (1997), Te97 = Tegler et al. (1997), Ro97 = Romanishin et al. (1997), JL98 = Jewitt & Luu (1998), MB99 = McBride et al. (1999), RT99 = Romanishin & Tegler (1999), Ba00 = Barucci et al. (2000), Da00 = Davies et al. (2000), TR00 = Tegler & Romanishin (2000), Bo01 = Boehnhardt et al. (2001), De01 = Delsanti et al. (2001), Do01 = Doressoundiram et al. (2001), Fe01 = Ferrin et al. (2001), GH01 = Gil-Hutton & Licandro (2001), JL01 = Jewitt & Luu (2001), Pe01 = Peixinho et al. (2001), Ba02 = Barucci et al. (2002), Bo02 = Boehnhardt et al. (2002), Do02 = Doressoundiram et al. (2002), Du02 = Duffard et al. (2002), Je02 = Jewitt (2002), JS02 = Jewitt & Sheppard (2002), RM02 = Romon-Martin et al. (2002), SR02 = Schaefer & Rabinowitz (2002), FD03 = Farnham & Davies (2003), MB03 = McBride et al. (2003), Do03 = Dotto et al. (2003), TR03 = Tegler & Romanishin (2003), Te03 = Tegler et al. (2003), Fo04 = Fornasier et al. (2004), Or04 = Ortiz et al. (2004), Px04 = Peixinho et al. (2004), Ba05 = Barucci et al. (2005), dB05 = de Bergh et al. (2005), Do05 = Doressoundiram et al. (2005), Ca06 = Carraro et al. (2006), Ra07 = Rabinowitz et al. (2007), DM09 = DeMeo et al. (2009), SS09 = Santos-Sanz et al. (2009), Be10 = Belskaya et al. (2010), Pe10 = Perna et al. (2010), Ro10 = Romanishin et al. (2010), Sh10 = Sheppard (2010), Sn10 = Snodgrass et al. (2010), Px12 = Peixinho et al. (2012), Pe13 = Perna et al. (2013), PA13 = Pinilla-Alonso et al. (2013), Bo14 = Böhnhardt et al. (2014), Fo14 = Fornasier et al. (2014), **TW** = This work.

Table A.2. continued.

Object	H_V	β (mag per degree)	N	Δm	References
55636 2002 TX_{300}	3.574 ± 0.055	0.005 ± 0.044	37	0.09	Ra07,Te03,Or04,Do05
55637 2002 UX_{25}	3.883 ± 0.048	0.159 ± 0.056	42	0.21	Ra07,SS09,DM09,**TW**
55638 2002 VE_{95}	5.813 ± 0.037	0.089 ± 0.024	43	0.08	Pe10,Ra07,**TW**
127546 2002 XU_{93}	7.031 ± 0.859	0.498 ± 0.320	5	–	Sh10,**TW**
208996 2003 AZ_{84}	3.779 ± 0.114	0.074 ± 0.118	5	0.14	DM09,Pe10,Fo04,SS09,Bo14
120061 2003 CO_1	9.146 ± 0.056	0.092 ± 0.015	5	0.07	Pe10,Pe13,Te03
133067 2003 FB_{128}	6.922 ± 0.566	0.422 ± 0.469	3	–	Pe13,Bo14
2003 FE_{128}	7.381 ± 0.256	−0.349 ± 0.209	5	–	Pe13,Bo14
120132 2003 FY_{128}	4.632 ± 0.187	0.535 ± 0.145	7	0.15	Pe10,Sh10,DM09,Bo14,**TW**
385437 2003 GH_{55}	7.319 ± 0.247	−0.880 ± 0.251	3	–	Pe13,Bo14
120178 2003 OP_{32}	4.067 ± 0.318	0.045 ± 0.280	11	0.26	Pe10,Bo14,Pe13,**TW**
143707 2003 UY_{117}	5.830 ± 1.299	−0.230 ± 1.329	3	–	**TW**
2003 UZ_{117}	5.185 ± 0.054	0.214 ± 0.073	3	–	Pe10,Bo14,DM09
2003 UZ_{413}	4.361 ± 0.068	0.144 ± 0.096	3	–	Pe10
136204 2003 WL_7	8.897 ± 0.149	0.089 ± 0.049	4	0.05	Pe13,**TW**
120216 2004 EW_{95}	6.579 ± 0.021	0.071 ± 0.024	4	–	Bo14,Pe13,**TW**
90568 2004 GV_9	3.409 ± 0.357	1.353 ± 0.542	3	0.16	Bo14,DM09,**TW**
307982 2004 PG_{115}	4.874 ± 0.064	0.505 ± 0.051	8	–	Pe13,Bo14,**TW**
120348 2004 TY_{364}	4.519 ± 0.137	0.146 ± 0.103	32	0.22	Ra07,Pe10
144897 2004 UX_{10}	4.825 ± 0.097	0.061 ± 0.103	8	0.08	Ro10,Pe10,**TW**
230965 2004 XA_{192}	5.059 ± 0.085	−0.175 ± 0.070	5	0.07	**TW**
303775 2005 QU_{182}	3.853 ± 0.028	0.277 ± 0.034	5	–	Pe13,Bo14,**TW**
145451 2005 RM_{43}	4.704 ± 0.081	−0.028 ± 0.064	6	0.04	Bo14,DM09,**TW**
145452 2005 RN_{43}	3.882 ± 0.036	0.138 ± 0.030	10	0.04	DM09,Pe13,**TW**
145453 2005 RR_{43}	4.252 ± 0.067	−0.003 ± 0.065	5	0.06	Pe10,DM09,**TW**
145480 2005 TB_{190}	4.676 ± 0.084	0.052 ± 0.106	7	0.12	Bo14,Pe13,**TW**
145486 2005 UJ_{438}	14.602 ± 0.617	−0.412 ± 0.098	5	0.13	Bo14,Pe13,**TW**
2007 OC_{10}	5.330 ± 0.825	0.223 ± 0.740	3	–	Pe13,**TW**
225088 2007 OR_{10}	2.316 ± 0.124	0.257 ± 0.505	7	–	Bo14,**TW**
281371 2008 FC_{76}	9.486 ± 0.078	0.101 ± 0.016	4	–	Pe10,Px12,Pe13
342842 2008 YB_3	11.024 ± 0.696	−0.104 ± 0.095	3	0.20	Pa13,Sh10,**TW**
55576 Amycus	8.213 ± 0.621	0.052 ± 0.351	3	0.16	Px04,Fo04,Pe10
8405 Asbolus	9.138 ± 0.130	0.042 ± 0.029	43	0.55	Ro97,BL97,Ra07,RM02
54598 Bienor	7.656 ± 0.443	0.130 ± 0.170	57	0.75	Ra07,DM09,Do02,Te03,De01
66652 Borasisi	6.032 ± 0.040	0.231 ± 0.062	3	0.05	Do01,MB03
65489 Ceto	6.573 ± 0.126	0.196 ± 0.096	8	0.13	Bo14,Te03,Pe13,**TW**
19521 Chaos	4.987 ± 0.065	0.102 ± 0.070	6	0.10	De01,TR00,Do02,Bo01,Da00,Ba00
10199 Chariklo	6.870 ± 0.055	0.064 ± 0.016	22	0.10	Pe01,Be10,DM09,Fo14,RT99,MB99,JL01,Pe10,**TW**
2060 Chiron	6.399 ± 0.019	0.083 ± 0.005	37	0.09	Be10,Du02,Je02,**TW**
83982 Crantor	9.096 ± 0.405	0.110 ± 0.149	5	0.34	Px04,DM09,Fo04,Te03
52975 Cyllarus	9.064 ± 0.041	0.184 ± 0.029	4	–	De01,Te03,Do02,Bo01
31824 Elatus	10.592 ± 0.171	0.078 ± 0.031	6	0.24	TR03,De01,Do02,Pe01
136199 Eris	−1.124 ± 0.025	0.119 ± 0.056	79	0.10	DM09,Ra07,Ca06,
38628 Huya	4.975 ± 0.037	0.173 ± 0.026	98	0.10	Fe01,SR02,TR03,Bo02,MB03,Do01,JL01
28978 Ixion	3.774 ± 0.021	0.194 ± 0.031	40	0.05	Ra07,DM09,Do02
58534 Logos	7.411 ± 0.041	0.055 ± 0.057	5	–	Ba00,GH01,JL01,Bo01
136472 Makemake	0.009 ± 0.012	0.202 ± 0.015	55	0.03	Ra07,**TW**
52872 Okyrhoe	11.441 ± 0.062	−0.023 ± 0.017	6	0.07	Do03,De01,Pe10,TR03,Bo14,Do01
90482 Orcus	2.280 ± 0.021	0.160 ± 0.022	30	0.04	Ra07,Pe10,dB05
49036 Pelion	10.911 ± 0.069	−0.074 ± 0.026	3	–	Do02,Bo02,TR00
5145 Pholus	7.474 ± 0.309	0.153 ± 0.156	15	0.60	Mu92,BB92,Be10,Ro97,**TW**
50000 Quaoar	2.777 ± 0.250	0.117 ± 0.221	45	0.30	Ra07,Te03,DM09,Fo04
120347 Salacia	4.151 ± 0.030	0.132 ± 0.028	9	0.03	Sn10,Bo14,Pe13,**TW**
90377 Sedna	1.669 ± 0.004	0.266 ± 0.008	170	0.02	Ra07,Ba05,Sh10,Pe10
79360 Sila-Nunam	5.573 ± 0.224	0.095 ± 0.209	6	0.22	Da00,Bo01,Ba00,JL01,RT99
32532 Thereus	9.454 ± 0.137	0.061 ± 0.034	67	0.34	Ra07,Te03,FD03,DM09,Ba02
42355 Typhon	7.670 ± 0.026	0.128 ± 0.013	22	0.07	Ra07,Te03,DM09,Pe10,Px04,**TW**
174567 Varda	3.988 ± 0.048	−0.455 ± 0.071	9	0.06	Bo14,Pe13,Pe10,**TW**
20000 Varuna	3.966 ± 0.233	0.104 ± 0.246	30	0.50	Ra07,Do02,Pe10,JS02,TR03

Table A.3. Comparison between the values of H_V and β from this work with those from three selected references.

	This work		Ra07		Pe13		Bo13
Object	H_V	β (mag per degree)	H_V	β (mag per degree)	H_V	β (mag per degree)	H_V
1999 DE_9	5.120 ± 0.024	0.183 ± 0.032	5.103 ± 0.029	0.209 ± 0.035			
1999 TC_{36}	5.395 ± 0.030	0.111 ± 0.027	5.272 ± 0.055	0.131 ± 0.049			
1999 TD_{10}	9.105 ± 0.430	0.033 ± 0.122	8.793 ± 0.029	0.150 ± 0.014			
2000 GN_{171}	6.776 ± 0.243	−0.101 ± 0.186	6.368 ± 0.034	0.143 ± 0.030			
2002 AW_{197}	3.593 ± 0.023	0.206 ± 0.029	3.568 ± 0.030	0.128 ± 0.040			
2002 GZ_{32}	7.419 ± 0.126	0.043 ± 0.064	7.389 ± 0.059	-0.025 ± 0.041			
2002 KX_{14}	4.978 ± 0.017	0.114 ± 0.031	4.862 ± 0.038	0.159 ± 0.044			5.07 ± 0.03
2002 KY_{14}	11.808 ± 0.763	−0.274 ± 0.193					10.50 ± 0.08
2002 PN_{34}	8.618 ± 0.054	0.090 ± 0.027	8.660 ± 0.017	0.043 ± 0.005			
2002 TX_{300}	3.574 ± 0.055	0.005 ± 0.044	3.365 ± 0.044	0.158 ± 0.053			
2002 UX_{25}	3.883 ± 0.048	0.159 ± 0.056	3.873 ± 0.020	0.158 ± 0.025			
2002 VE_{95}	5.813 ± 0.037	0.089 ± 0.024	5.748 ± 0.058	0.121 ± 0.039			
2003 AZ_{84}	3.779 ± 0.114	0.074 ± 0.118					3.54 ± 0.03
2003 CO_1	9.146 ± 0.056	0.092 ± 0.015			9.07 ± 0.05	0.09 ± 0.01	
2003 FB_{128}	6.922 ± 0.566	0.422 ± 0.469			7.09 ± 0.20		7.26 ± 0.05
2003 FE_{128}	7.381 ± 0.256	−0.349 ± 0.209			6.74 ± 0.18		6.94 ± 0.07
2003 FY_{128}	4.632 ± 0.187	0.535 ± 0.145					5.36 ± 0.08
2003 GH_{55}	7.319 ± 0.247	−0.880 ± 0.251			6.32 ± 0.13		**6.18 ± 0.04**
2003 OP_{32}	4.067 ± 0.318	0.045 ± 0.280			3.99 ± 0.11	0.05 ± 0.08	3.79 ± 0.08
2003 UZ_{117}	5.185 ± 0.054	0.214 ± 0.073					5.27 ± 0.02
2003 WL_7	8.897 ± 0.149	0.089 ± 0.049			8.75 ± 0.16		
2004 EW_{95}	6.579 ± 0.021	0.071 ± 0.024			6.39 ± 0.15		6.52 ± 0.01
2004 GV_9	3.409 ± 0.357	1.353 ± 0.542					4.03 ± 0.03
2004 PG_{115}	4.874 ± 0.064	0.505 ± 0.051			5.23 ± 0.15		**5.53 ± 0.05**
2004 TY_{364}	4.519 ± 0.137	0.146 ± 0.103	4.434 ± 0.074	0.184 ± 0.070			
2005 QU_{182}	3.853 ± 0.028	0.277 ± 0.034			3.82 ± 0.12		3.99 ± 0.02
2005 RM_{43}	4.704 ± 0.081	−0.028 ± 0.064					4.52 ± 0.01
2005 RN_{43}	3.882 ± 0.036	0.138 ± 0.030			3.72 ± 0.05	0.18 ± 0.03	
2005 TB_{190}	4.676 ± 0.084	0.052 ± 0.106			4.62 ± 0.15		4.56 ± 0.02
2005 UJ_{438}	14.602 ± 0.617	−0.412 ± 0.098			**11.14 ± 0.32**		
2007 OC_{10}	5.330 ± 0.825	0.223 ± 0.740			5.36 ± 0.13		
2007 OR_{10}	2.316 ± 0.124	0.257 ± 0.505					2.34 ± 0.01
2008 FC_{76}	9.486 ± 0.078	0.101 ± 0.016			9.43 ± 0.13	0.09 ± 0.02	
Asbolus	9.138 ± 0.130	0.042 ± 0.029	9.107 ± 0.016	0.050 ± 0.004			
Bienor	7.656 ± 0.443	0.130 ± 0.170	7.588 ± 0.035	0.095 ± 0.016			
Ceto	6.573 ± 0.126	0.196 ± 0.096			6.58 ± 0.10	0.10 ± 0.06	6.60 ± 0.01
Eris	−1.124 ± 0.025	0.119 ± 0.056	-1.116 ± 0.009	0.105 ± 0.020			
Huya	5.015 ± 0.021	0.124 ± 0.015	5.048 ± 0.005	0.155 ± 0.041			
Ixion	3.774 ± 0.021	0.194 ± 0.031	3.766 ± 0.042	0.133 ± 0.043			
Makemake	0.009 ± 0.012	0.202 ± 0.015	**0.091 ± 0.015**	**0.054 ± 0.019**			
Okyrhoe	11.441 ± 0.062	−0.023 ± 0.017					**10.83 ± 0.01**
Orcus	2.280 ± 0.021	0.160 ± 0.022	2.328 ± 0.028	0.114 ± 0.030			
Quaoar	2.777 ± 0.250	0.117 ± 0.221	2.729 ± 0.025	0.159 ± 0.027			
Salacia	4.151 ± 0.030	0.132 ± 0.028			4.26 ± 0.06	0.04 ± 0.06	4.01 ± 0.02
Sedna	1.443 ± 0.003	0.200 ± 0.006	**1.829 ± 0.048**				
Thereus	9.454 ± 0.137	0.061 ± 0.034	9.417 ± 0.014	0.072 ± 0.004			
Typhon	7.670 ± 0.026	0.128 ± 0.013	7.676 ± 0.037	0.126 ± 0.022			
Varda	3.988 ± 0.048	−0.455 ± 0.071			**3.51 ± 0.06**		3.93 ± 0.07
Varuna	3.966 ± 0.233	0.104 ± 0.246	3.760 ± 0.032	0.278 ± 0.047			

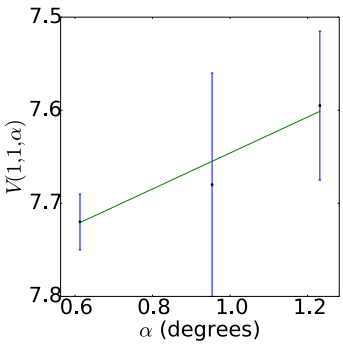

Fig. A.1. Phase curve of 15 760 1992 QB_1. The continuous line indicate the best fit to Eq. (5) resulting in $H_V = 7.839 \pm 0.097$, $\beta = (-0.193 \pm 0.132)$ mag per degree.

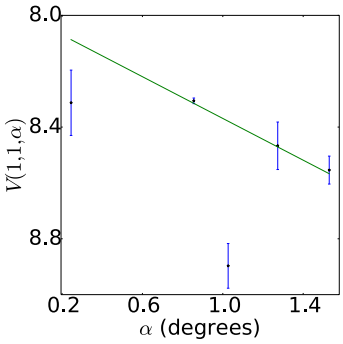

Fig. A.2. Phase curve of 15 788 1993 SB. The continuous line indicate the best fit to Eq. (5) resulting in $H_V = 7.995 \pm 0.059$, $\beta = (0.374 \pm 0.066)$ mag per degree.

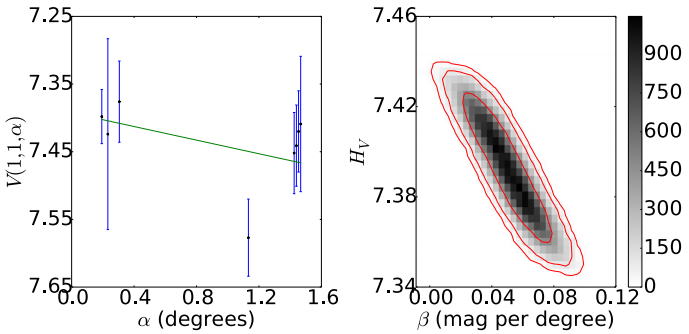

Fig. A.3. *Left*: phase curve of 15 789 1993 SC. The continuous line indicate the best fit to Eq. (5) resulting in $H_V = 7.393 \pm 0.020$, $\beta = (0.050 \pm 0.017)$ mag per degree. *Right*: density plot showing the phase space of solutions of Eq. (5) for $\Delta m = 0.04$, in gray scale. The continuous lines show the area that contain 68.3, 95.5, and 99.7% of the solutions.

Fig. A.4. Phase curve of 1994 EV_3. The continuous line indicate the best fit to Eq. (5) resulting in $H_V = 8.183 \pm 0.247$, $\beta = (-0.803 \pm 0.329)$ mag per degree.

Fig. A.5. Phase curve of 16 684 1994 JQ_1. The continuous line indicate the best fit to Eq. (5) resulting in $H_V = 7.031 \pm 0.078$, $\beta = (0.570 \pm 0.125)$ mag per degree.

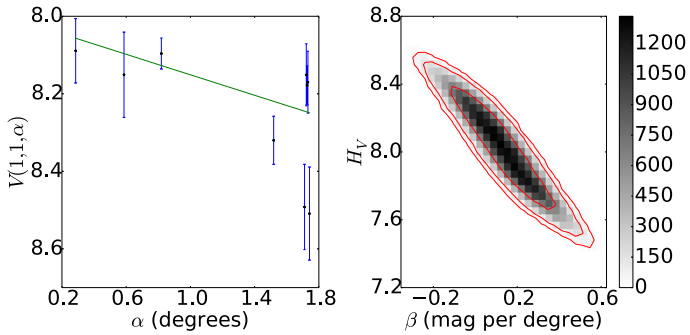

Fig. A.6. *Left*: phase curve of 15 820 1994 TB. The continuous line indicate the best fit to Eq. (5) resulting in $H_V = 8.017 \pm 0.226$, $\beta = (0.133 \pm 0.152)$ mag per degree. *Right*: density plot showing the phase space of solutions of Eq. (5) for $\Delta m = 0.34$, in gray scale. The continuous lines show the area that contain 68.3, 95.5, and 99.7% of the solutions.

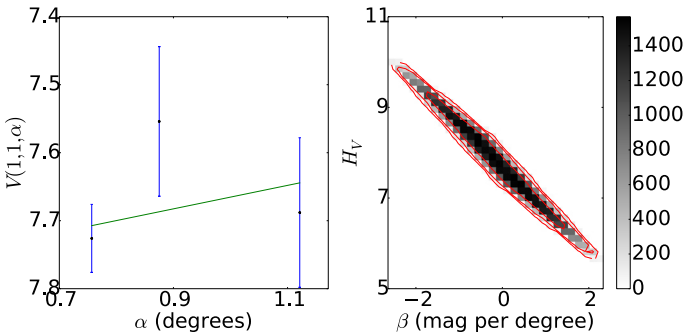

Fig. A.7. *Left*: phase curve of 19 255 1994 VK_8. The continuous line indicate the best fit to Eq. (5) resulting in $H_V = 7.840 \pm 0.923$, $\beta = (-0.173 \pm 0.976)$ mag per degree. *Right*: density plot showing the phase space of solutions of Eq. (5) for $\Delta m = 0.42$, in gray scale. The continuous lines show the area that contain 68.3, 95.5, and 99.7% of the solutions.

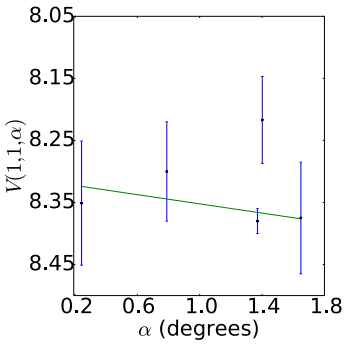

Fig. A.8. Phase curve of 1995 HM_5. The continuous line indicate the best fit to Eq. (5) resulting in $H_V = 8.315 \pm 0.100$, $\beta = (0.037 \pm 0.074)$ mag per degree.

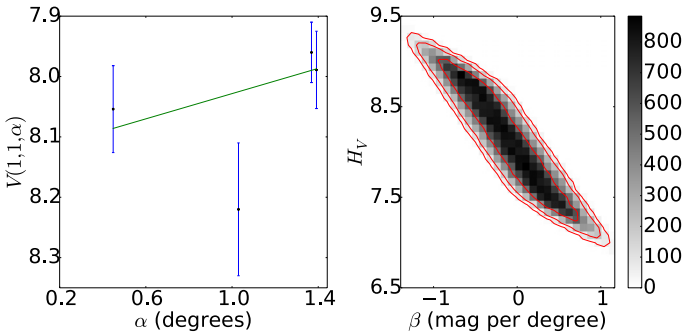

Fig. A.9. *Left*: phase curve of 32 929 1995 QY_9. The continuous line indicate the best fit to Eq. (5) resulting in $H_V = 8.136 \pm 0.515$, $\beta = (-0.108 \pm 0.459)$ mag per degree. *Right*: density plot showing the phase space of solutions of Eq. (5) for $\Delta m = 0.60$, in gray scale. The continuous lines show the area that contain 68.3, 95.5, and 99.7% of the solutions.

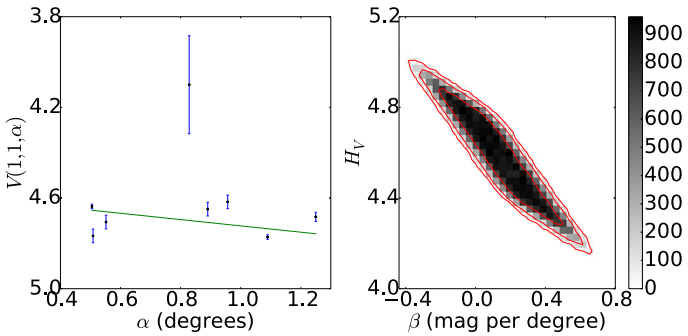

Fig. A.10. *Left*: phase curve of 24 835 1995 SM_{55}. The continuous line indicate the best fit to Eq. (5) resulting in $H_V = 4.584 \pm 0.178$, $\beta = (0.139 \pm 0.198)$ mag per degree. *Right*: density plot showing the phase space of solutions of Eq. (5) for $\Delta m = 0.19$, in gray scale. The continuous lines show the area that contain 68.3, 95.5, and 99.7% of the solutions.

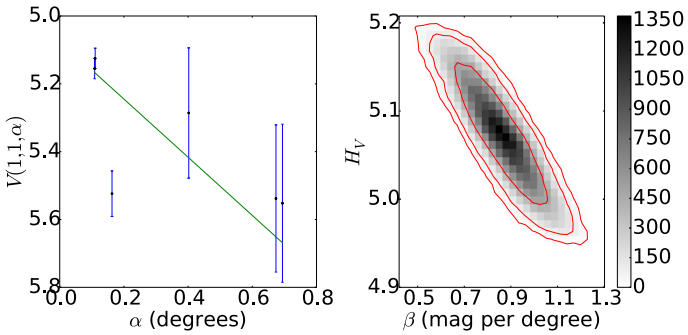

Fig. A.11. *Left*: phase curve of 26181 1996 GQ_{21}. The continuous line indicate the best fit to Eq. (5) resulting in $H_V = 5.073 \pm 0.050$, $\beta = (0.858 \pm 0.124)$ mag per degree. *Right*: density plot showing the phase space of solutions of Eq. (5) for $\Delta m = 0.10$, in gray scale. The continuous lines show the area that contain 68.3, 95.5, and 99.7% of the solutions.

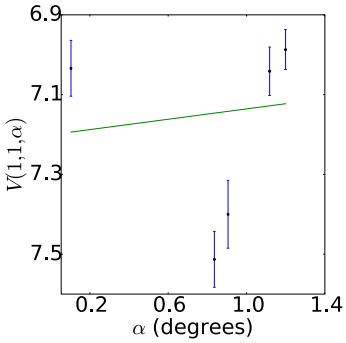

Fig. A.12. Phase curve of 1996 RQ_{20}. The continuous line indicate the best fit to Eq. (5) resulting in $H_V = 7.201 \pm 0.073$, $\beta = (-0.065 \pm 0.075)$ mag per degree.

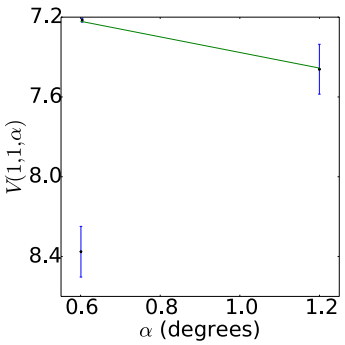

Fig. A.13. Phase curve of 1996 RR_{20}. The continuous line indicate the best fit to Eq. (5) resulting in $H_V = 6.986 \pm 0.128$, $\beta = (0.391 \pm 0.210)$ mag per degree.

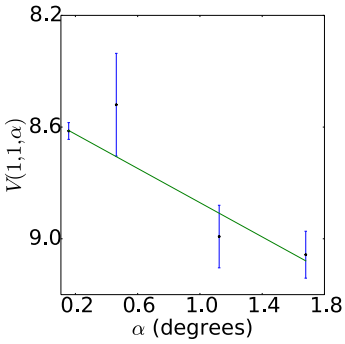

Fig. A.14. Phase curve of 19 299 1996 SZ_4. The continuous line indicate the best fit to Eq. (5) resulting in $H_V = 8.564 \pm 0.034$, $\beta = (0.307 \pm 0.054)$ mag per degree.

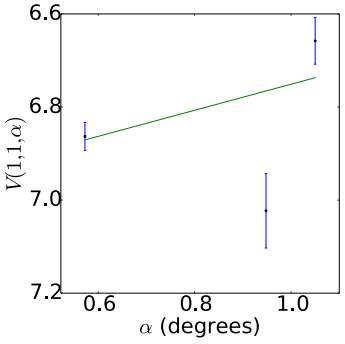

Fig. A.15. Phase curve of 1996 TK_{66}. The continuous line indicate the best fit to Eq. (5) resulting in $H_V = 7.031 \pm 0.086$, $\beta = (-0.280 \pm 0.115)$ mag per degree.

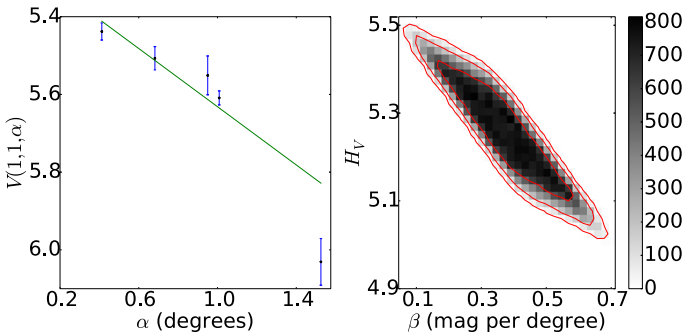

Fig. A.16. *Left*: phase curve of 15 874 1996 TL_{66}. The continuous line indicate the best fit to Eq. (5) resulting in $H_V = 5.257 \pm 0.100$, $\beta = (0.375 \pm 0.112)$ mag per degree. *Right*: density plot showing the phase space of solutions of Eq. (5) for $\Delta m = 0.12$, in gray scale. The continuous lines show the area that contain 68.3, 95.5, and 99.7% of the solutions.

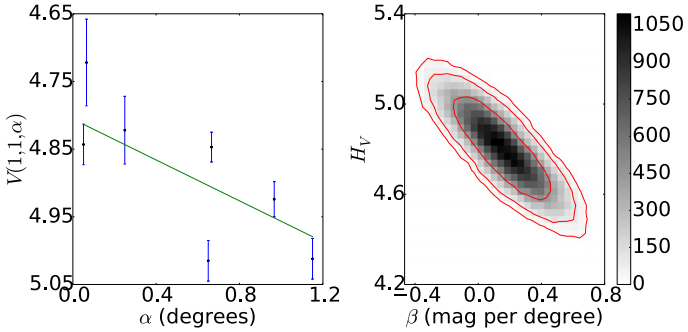

Fig. A.17. *Left*: phase curve of 19 308 1996 TO_{66}. The continuous line indicate the best fit to Eq. (5) resulting in $H_V = 4.806 \pm 0.144$, $\beta = (0.150 \pm 0.197)$ mag per degree. *Right*: density plot showing the phase space of solutions of Eq. (5) for $\Delta m = 0.33$, in gray scale. The continuous lines show the area that contain 68.3, 95.5, and 99.7% of the solutions.

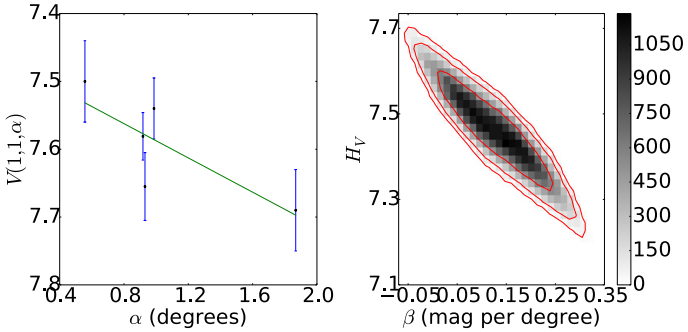

Fig. A.18. *Left*: phase curve of 15 875 1996 TP_{66}. The continuous line indicate the best fit to Eq. (5) resulting in $H_V = 7.461 \pm 0.084$, $\beta = (0.127 \pm 0.072)$ mag per degree. *Right*: density plot showing the phase space of solutions of Eq. (5) for $\Delta m = 0.12$, in gray scale. The continuous lines show the area that contain 68.3, 95.5, and 99.7% of the solutions.

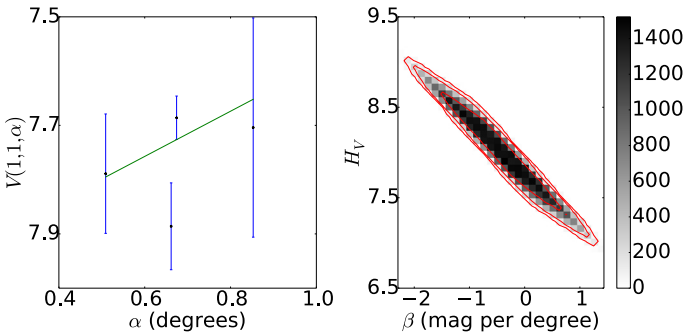

Fig. A.19. *Left*: phase curve of 118 228 1996 TQ_{66}. The continuous line indicate the best fit to Eq. (5) resulting in $H_V = 8.006 \pm 0.422$, $\beta = (-0.415 \pm 0.680)$ mag per degree. *Right*: density plot showing the phase space of solutions of Eq. (5) for $\Delta m = 0.22$, in gray scale. The continuous lines show the area that contain 68.3, 95.5, and 99.7% of the solutions.

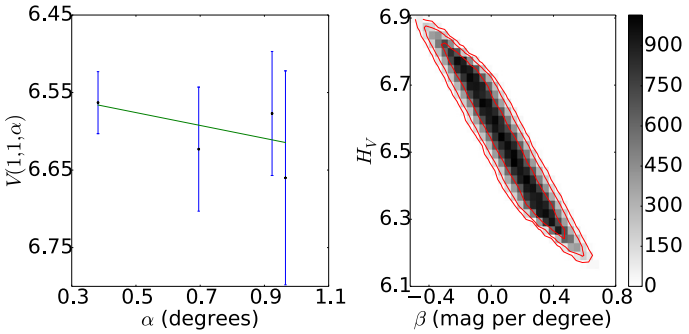

Fig. A.20. *Left*: phase curve of 1996 TS_{66}. The continuous line indicate the best fit to Eq. (5) resulting in $H_V = 6.535 \pm 0.167$, $\beta = (0.083 \pm 0.220)$ mag per degree. *Right*: density plot showing the phase space of solutions of Eq. (5) for $\Delta m = 0.16$, in gray scale. The continuous lines show the area that contain 68.3, 95.5, and 99.7% of the solutions.

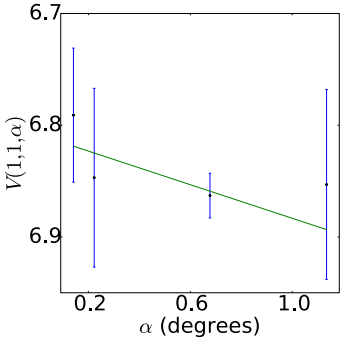

Fig. A.21. Phase curve of 33 001 1997 CU_{29}. The continuous line indicate the best fit to Eq. (5) resulting in $H_V = 6.808 \pm 0.057$, $\beta = (0.075 \pm 0.087)$ mag per degree.

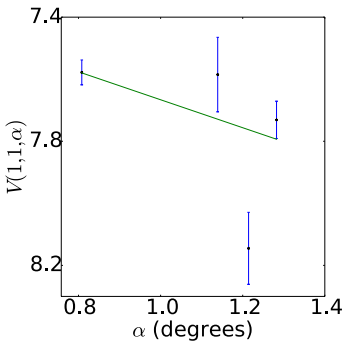

Fig. A.22. Phase curve of 1997 QH_4. The continuous line indicate the best fit to Eq. (5) resulting in $H_V = 7.216 \pm 0.143$, $\beta = (0.451 \pm 0.142)$ mag per degree.

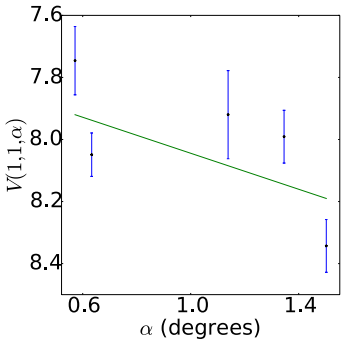

Fig. A.23. Phase curve of 1997 QJ_4. The continuous line indicate the best fit to Eq. (5) resulting in $H_V = 7.754 \pm 0.113$, $\beta = (0.290 \pm 0.103)$ mag per degree.

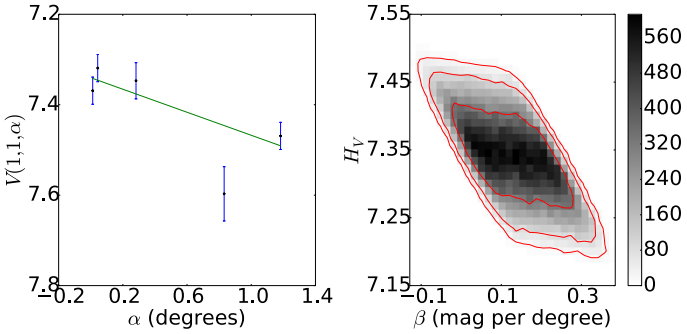

Fig. A.24. *Left*: phase curve of 91 133 1998 HK_{151}. The continuous line indicate the best fit to Eq. (5) resulting in $H_V = 7.340 \pm 0.056$, $\beta = (0.127 \pm 0.088)$ mag per degree. *Right*: density plot showing the phase space of solutions of Eq. (5) for $\Delta m = 0.15$, in gray scale. The continuous lines show the area that contain 68.3, 95.5, and 99.7% of the solutions.

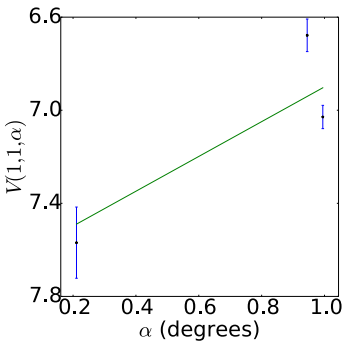

Fig. A.25. Phase curve of 385 194 1998 KG_{62}. The continuous line indicate the best fit to Eq. (5) resulting in $H_V = 7.647 \pm 0.194$, $\beta = (-0.748 \pm 0.205)$ mag per degree.

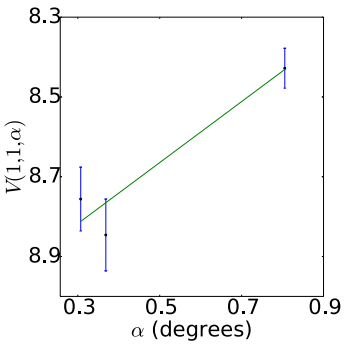

Fig. A.28. Phase curve of 1998 UR_{43}. The continuous line indicate the best fit to Eq. (5) resulting in $H_V = 9.047 \pm 0.108$, $\beta = (-0.764 \pm 0.165)$ mag per degree.

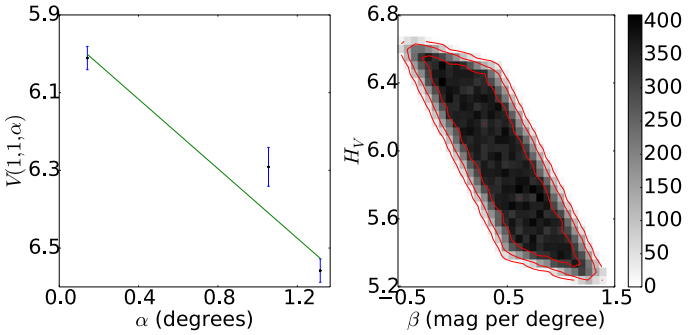

Fig. A.26. *Left*: phase curve of 26 308 1998 SM_{165}. The continuous line indicate the best fit to Eq. (5) resulting in $H_V = 5.938 \pm 0.363$, $\beta = (0.446 \pm 0.376)$ mag per degree. *Right*: density plot showing the phase space of solutions of Eq. (5) for $\Delta m = 0.56$, in gray scale. The continuous lines show the area that contain 68.3, 95.5, and 99.7% of the solutions.

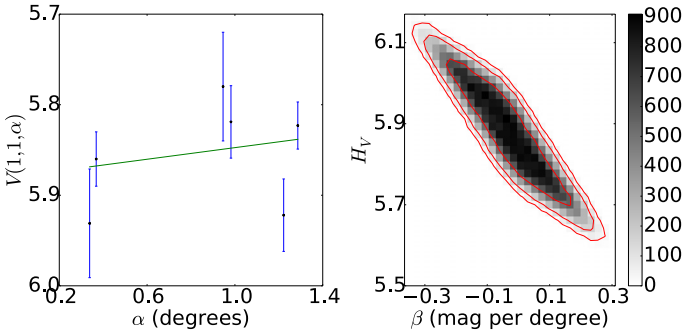

Fig. A.27. *Left*: phase curve of 35 671 1998 SN_{165}. The continuous line indicate the best fit to Eq. (5) resulting in $H_V = 5.879 \pm 0.109$, $\beta = (-0.031 \pm 0.115)$ mag per degree. *Right*: density plot showing the phase space of solutions of Eq. (5) for $\Delta m = 0.16$, in gray scale. The continuous lines show the area that contain 68.3, 95.5, and 99.7% of the solutions.

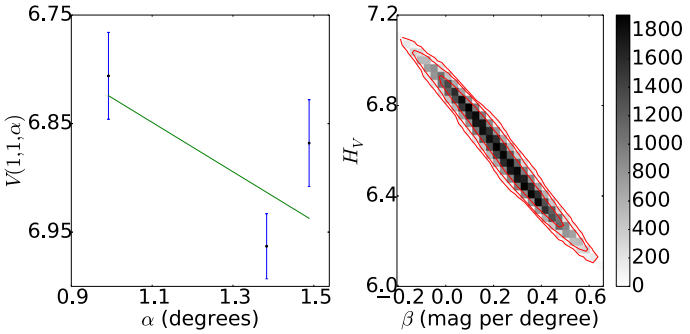

Fig. A.29. *Left*: phase curve of 33 340 1998 VG_{44}. The continuous line indicate the best fit to Eq. (5) resulting in $H_V = 6.599 \pm 0.205$, $\beta = (0.228 \pm 0.158)$ mag per degree. *Right*: density plot showing the phase space of solutions of Eq. (5) for $\Delta m = 0.10$, in gray scale. The continuous lines show the area that contain 68.3, 95.5, and 99.7% of the solutions.

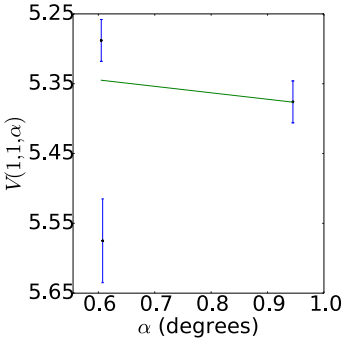

Fig. A.30. Phase curve of 1999 CD_{158}. The continuous line indicate the best fit to Eq. (5) resulting in $H_V = 5.289 \pm 0.092$, $\beta = (0.092 \pm 0.119)$ mag per degree.

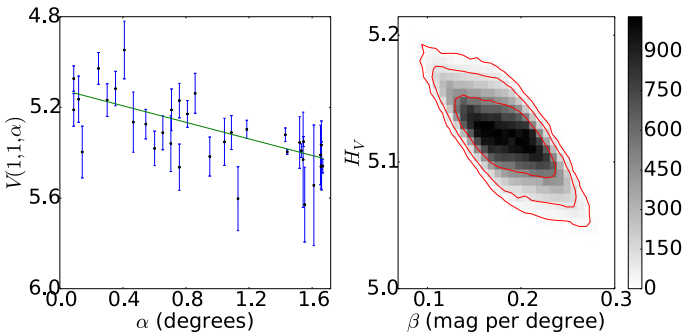

Fig. A.31. *Left*: phase curve of 26 375 1999 DE_9. The continuous line indicate the best fit to Eq. (5) resulting in $H_V = 5.120 \pm 0.024$, $\beta = (0.183 \pm 0.032)$ mag per degree. *Right*: density plot showing the phase space of solutions of Eq. (5) for $\Delta m = 0.10$, in gray scale. The continuous lines show the area that contain 68.3, 95.5, and 99.7% of the solutions.

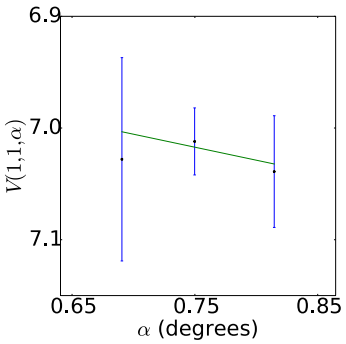

Fig. A.32. Phase curve of 1999 HS_{11}. The continuous line indicate the best fit to Eq. (5) resulting in $H_V = 6.843 \pm 0.555$, $\beta = (0.233 \pm 0.728)$ mag per degree.

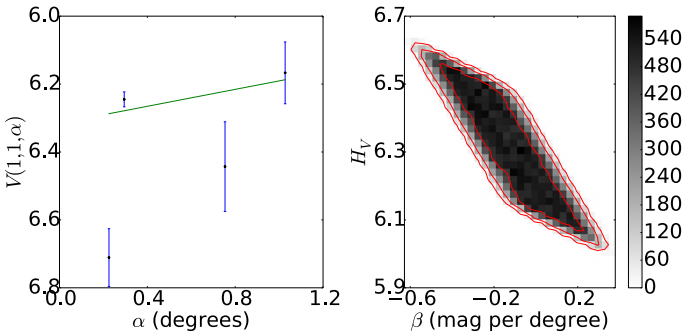

Fig. A.33. *Left*: phase curve of 40 314 1999 KR_{16}. The continuous line indicate the best fit to Eq. (5) resulting in $H_V = 6.316 \pm 0.139$, $\beta = (-0.126 \pm 0.180)$ mag per degree. *Right*: density plot showing the phase space of solutions of Eq. (5) for $\Delta m = 0.18$, in gray scale. The continuous lines show the area that contain 68.3, 95.5, and 99.7% of the solutions.

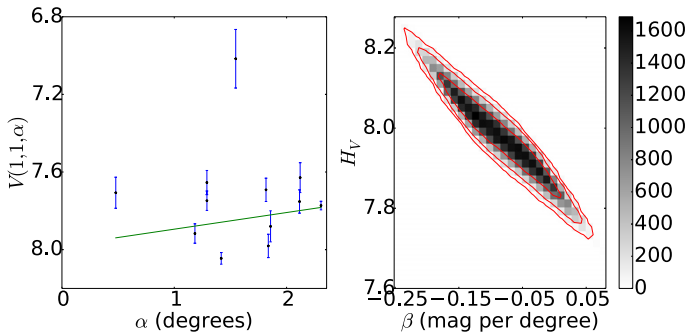

Fig. A.34. *Left*: phase curve of 44 594 1999 OX_3. The continuous line indicate the best fit to Eq. (5) resulting in $H_V = 7.980 \pm 0.092$, $\beta = (-0.086 \pm 0.057)$ mag per degree. *Right*: density plot showing the phase space of solutions of Eq. (5) for $\Delta m = 0.11$, in gray scale. The continuous lines show the area that contain 68.3, 95.5, and 99.7% of the solutions.

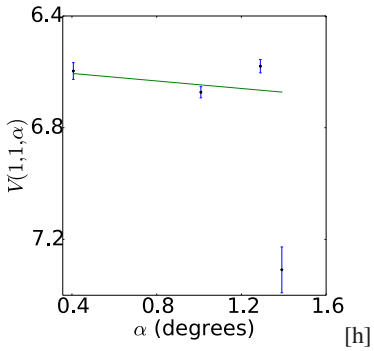

Fig. A.35. Phase curve of 86 047 1999 OY_3. The continuous line indicate the best fit to Eq. (5) resulting in $H_V = 6.579 \pm 0.044$, $\beta = (0.067 \pm 0.042)$ mag per degree.

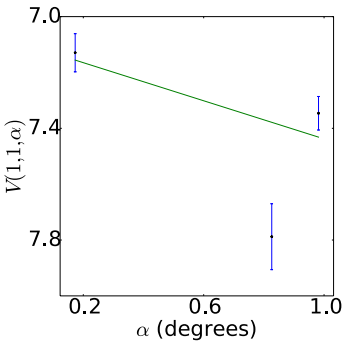

Fig. A.36. Phase curve of 86 177 1999 RY_{215}. The continuous line indicate the best fit to Eq. (5) resulting in $H_V = 7.097 \pm 0.084$, $\beta = (0.341 \pm 0.111)$ mag per degree.

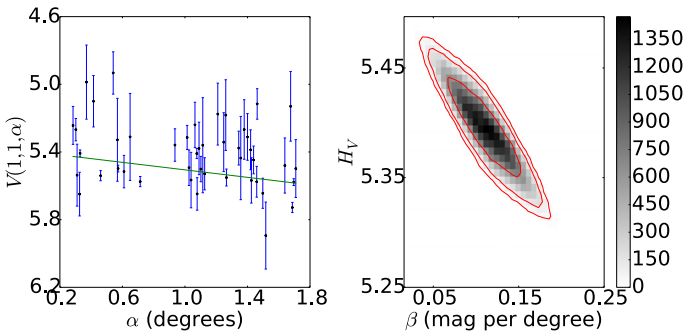

Fig. A.37. *Left*: phase curve of 47171 1999 TC_{36}. The continuous line indicate the best fit to Eq. (5) resulting in $H_V = 5.395 \pm 0.030$, $\beta = (0.111 \pm 0.027)$ mag per degree. *Right*: density plot showing the phase space of solutions of Eq. (5) for $\Delta m = 0.07$, in gray scale. The continuous lines show the area that contain 68.3, 95.5, and 99.7% of the solutions.

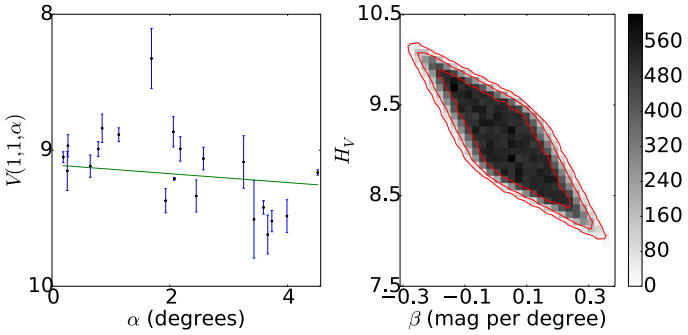

Fig. A.38. *Left*: phase curve of 29 981 1999 TD_{10}. The continuous line indicate the best fit to Eq. (5) resulting in $H_V = 9.105 \pm 0.430$, $\beta = (0.033 \pm 0.122)$ mag per degree. *Right*: density plot showing the phase space of solutions of Eq. (5) for $\Delta m = 0.65$, in gray scale. The continuous lines show the area that contain 68.3, 95.5, and 99.7% of the solutions.

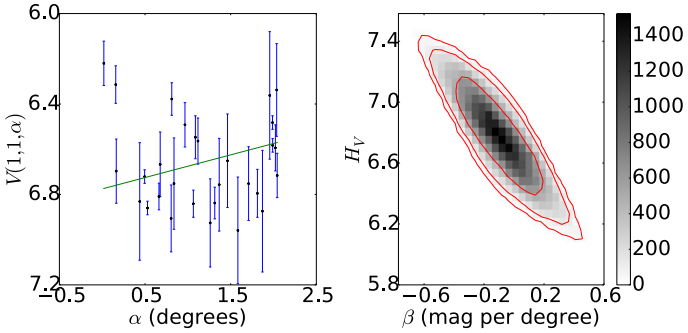

Fig. A.39. *Left*: phase curve of 47 932 2000 GN_{171}. The continuous line indicate the best fit to Eq. (5) resulting in $H_V = 6.776 \pm 0.243$, $\beta = (-0.101 \pm 0.186)$ mag per degree. *Right*: density plot showing the phase space of solutions of Eq. (5) for $\Delta m = 0.61$, in gray scale. The continuous lines show the area that contain 68.3, 95.5, and 99.7% of the solutions.

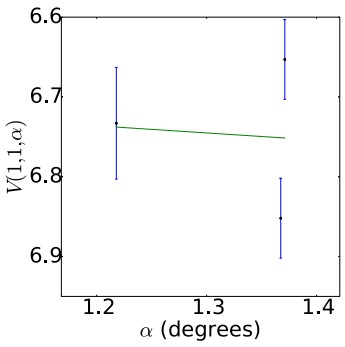

Fig. A.40. Phase curve of 138 537 2000 OK_{67}. The continuous line indicate the best fit to Eq. (5) resulting in $H_V = 6.629 \pm 0.694$, $\beta = (0.089 \pm 0.518)$ mag per degree.

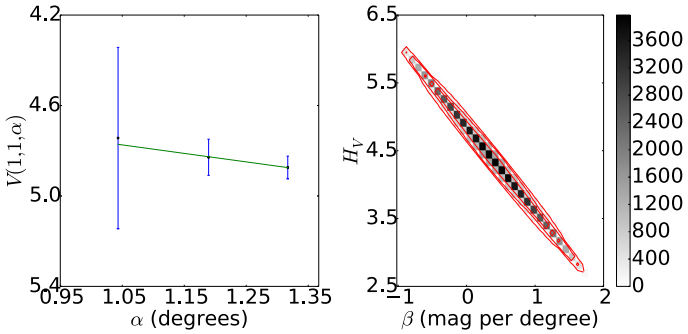

Fig. A.41. *Left*: phase curve of 82 075 2000 YW_{134}. The continuous line indicate the best fit to Eq. (5) resulting in $H_V = 4.378 \pm 0.687$, $\beta = (0.377 \pm 0.552)$ mag per degree. *Right*: density plot showing the phase space of solutions of Eq. (5) for $\Delta m = 0.10$, in gray scale. The continuous lines show the area that contain 68.3, 95.5, and 99.7% of the solutions.

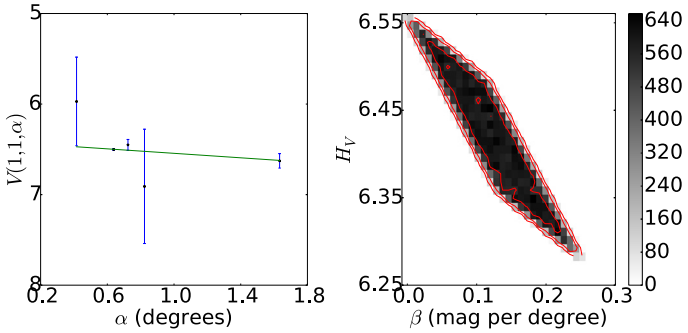

Fig. A.42. *Left*: phase curve of 82 158 2001 FP_{185}. The continuous line indicate the best fit to Eq. (5) resulting in $H_V = 6.420 \pm 0.062$, $\beta = (0.123 \pm 0.052)$ mag per degree. *Right*: density plot showing the phase space of solutions of Eq. (5) for $\Delta m = 0.06$, in gray scale. The continuous lines show the area that contain 68.3, 95.5, and 99.7% of the solutions.

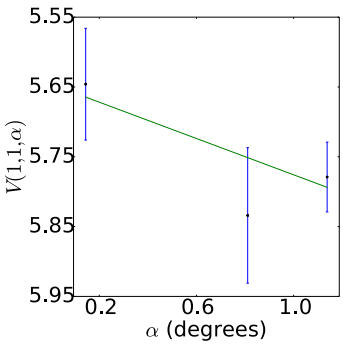

Fig. A.43. Phase curve of 2001 KA_{77}. The continuous line indicate the best fit to Eq. (5) resulting in $H_V = 5.646 \pm 0.090$, $\beta = (0.130 \pm 0.095)$ mag per degree.

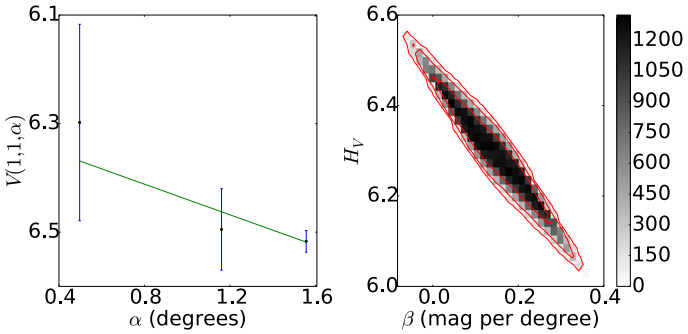

Fig. A.44. *Left*: phase curve of 2001 KD_{77}. The continuous line indicate the best fit to Eq. (5) resulting in $H_V = 6.299 \pm 0.099$, $\beta = (0.141 \pm 0.082)$ mag per degree. *Right*: density plot showing the phase space of solutions of Eq. (5) for $\Delta m = 0.07$, in gray scale. The continuous lines show the area that contain 68.3, 95.5, and 99.7% of the solutions.

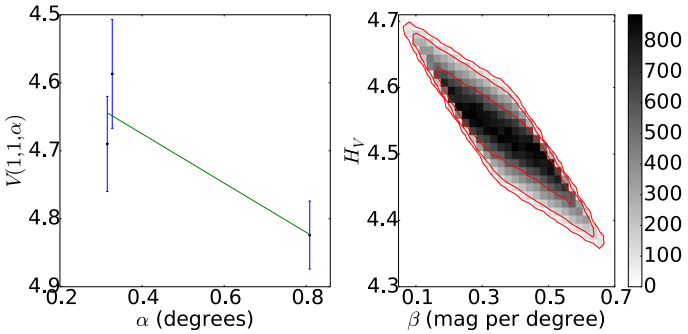

Fig. A.45. *Left*: phase curve of 42 301 2001 UR_{163}. The continuous line indicate the best fit to Eq. (5) resulting in $H_V = 4.529 \pm 0.063$, $\beta = (0.364 \pm 0.117)$ mag per degree. *Right*: density plot showing the phase space of solutions of Eq. (5) for $\Delta m = 0.08$, in gray scale. The continuous lines show the area that contain 68.3, 95.5, and 99.7% of the solutions.

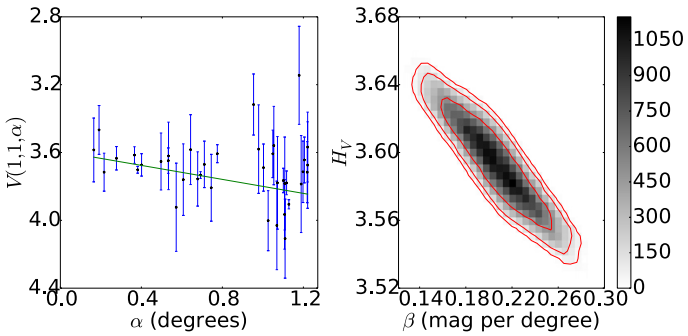

Fig. A.46. *Left*: phase curve of 55 565 2002 AW_{197}. The continuous line indicate the best fit to Eq. (5) resulting in $H_V = 3.593 \pm 0.023$, $\beta = (0.206 \pm 0.029)$ mag per degree. *Right*: density plot showing the phase space of solutions of Eq. (5) for $\Delta m = 0.04$, in gray scale. The continuous lines show the area that contain 68.3, 95.5, and 99.7% of the solutions.

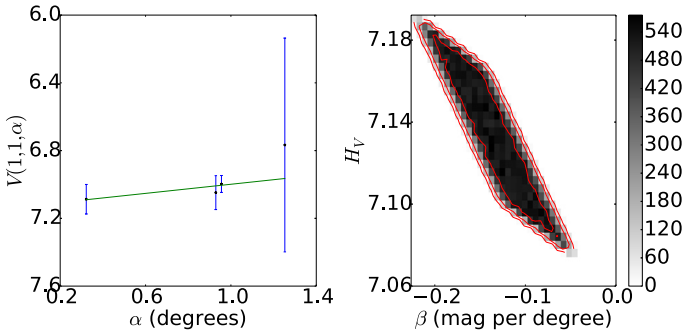

Fig. A.47. *Left*: phase curve of 2002 GP_{32}. The continuous line indicate the best fit to Eq. (5) resulting in $H_V = 7.133 \pm 0.027$, $\beta = (-0.135 \pm 0.036)$ mag per degree. *Right*: density plot showing the phase space of solutions of Eq. (5) for $\Delta m = 0.03$, in gray scale. The continuous lines show the area that contain 68.3, 95.5, and 99.7% of the solutions.

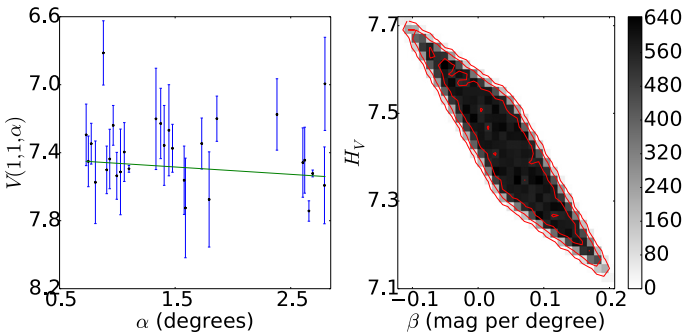

Fig. A.48. *Left*: phase curve of 95 626 2002 GZ_{32}. The continuous line indicate the best fit to Eq. (5) resulting in $H_V = 7.419 \pm 0.126$, $\beta = (0.043 \pm 0.064)$ mag per degree. *Right*: density plot showing the phase space of solutions of Eq. (5) for $\Delta m = 0.15$, in gray scale. The continuous lines show the area that contain 68.3, 95.5, and 99.7% of the solutions.

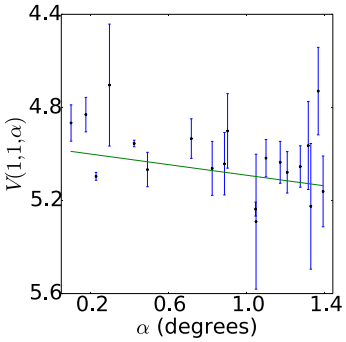

Fig. A.49. Phase curve of 119 951 2002 KX_{14}. The continuous line indicate the best fit to Eq. (5) resulting in $H_V = 4.978 \pm 0.017$, $\beta = (0.114 \pm 0.031)$ mag per degree.

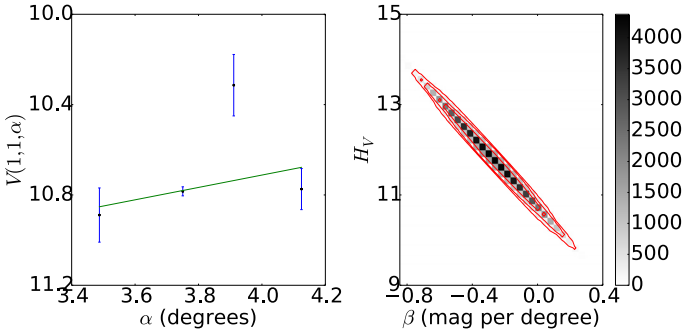

Fig. A.50. *Left*: phase curve of 250 112 2002 KY_{14}. The continuous line indicate the best fit to Eq. (5) resulting in $H_V = 11.808 \pm 0.763$, $\beta = (-0.274 \pm 0.193)$ mag per degree. *Right*: density plot showing the phase space of solutions of Eq. (5) for $\Delta m = 0.13$, in gray scale. The continuous lines show the area that contain 68.3, 95.5, and 99.7% of the solutions.

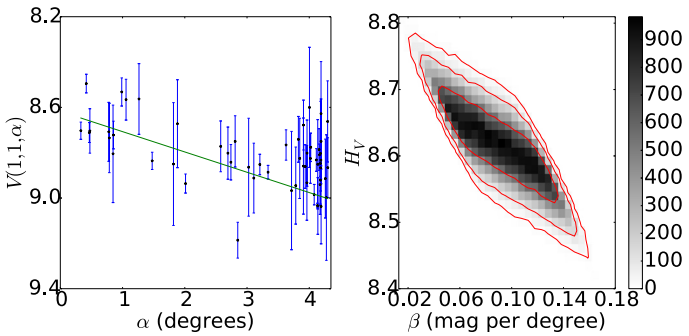

Fig. A.51. *Left*: phase curve of 73 480 2002 PN_{34}. The continuous line indicate the best fit to Eq. (5) resulting in $H_V = 8.618 \pm 0.054$, $\beta = (0.090 \pm 0.027)$ mag per degree. *Right*: density plot showing the phase space of solutions of Eq. (5) for $\Delta m = 0.18$, in gray scale. The continuous lines show the area that contain 68.3, 95.5, and 99.7% of the solutions.

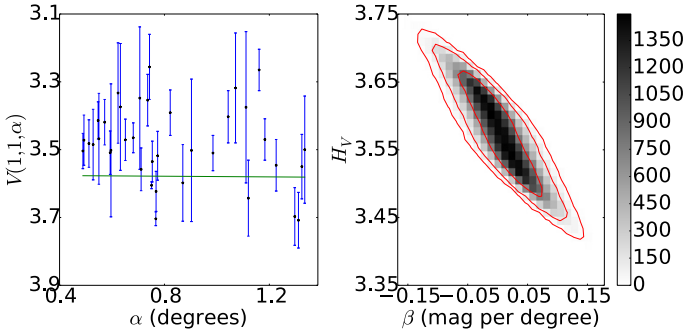

Fig. A.52. *Left*: phase curve of 55 636 2002 TX_{300}. The continuous line indicate the best fit to Eq. (5) resulting in $H_V = 3.574 \pm 0.055$, $\beta = (0.005 \pm 0.044)$ mag per degree. *Right*: density plot showing the phase space of solutions of Eq. (5) for $\Delta m = 0.09$, in gray scale. The continuous lines show the area that contain 68.3, 95.5, and 99.7% of the solutions.

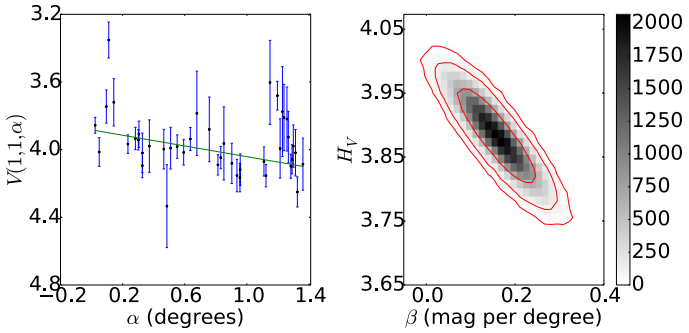

Fig. A.53. *Left*: phase curve of 55 637 2002 UX_{25}. The continuous line indicate the best fit to Eq. (5) resulting in $H_V = 3.883 \pm 0.048$, $\beta = (0.159 \pm 0.056)$ mag per degree. *Right*: density plot showing the phase space of solutions of Eq. (5) for $\Delta m = 0.21$, in gray scale. The continuous lines show the area that contain 68.3, 95.5, and 99.7% of the solutions.

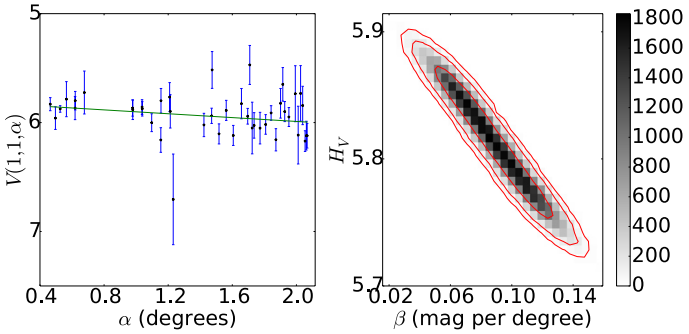

Fig. A.54. *Left*: phase curve of 55 638 2002 VE_{95}. The continuous line indicate the best fit to Eq. (5) resulting in $H_V = 5.813 \pm 0.037$, $\beta = (0.089 \pm 0.024)$ mag per degree. *Right*: density plot showing the phase space of solutions of Eq. (5) for $\Delta m = 0.08$, in gray scale. The continuous lines show the area that contain 68.3, 95.5, and 99.7% of the solutions.

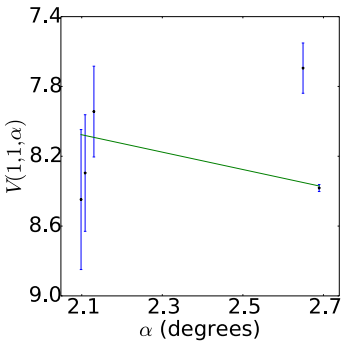

Fig. A.55. Phase curve of 127 546 2002 XU_{93}. The continuous line indicate the best fit to Eq. (5) resulting in $H_V = 7.031 \pm 0.859$, $\beta = (0.498 \pm 0.320)$ mag per degree.

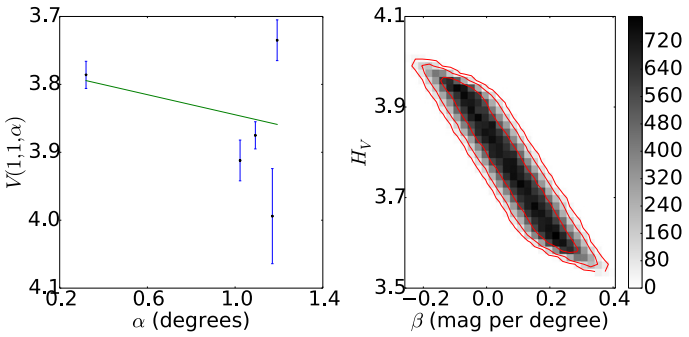

Fig. A.56. *Left*: phase curve of 208 996 2003 AZ_{84}. The continuous line indicate the best fit to Eq. (5) resulting in $H_V = 3.779 \pm 0.114$, $\beta = (0.054 \pm 0.118)$ mag per degree. *Right*: density plot showing the phase space of solutions of Eq. (5) for $\Delta m = 0.14$, in gray scale. The continuous lines show the area that contain 68.3, 95.5, and 99.7% of the solutions.

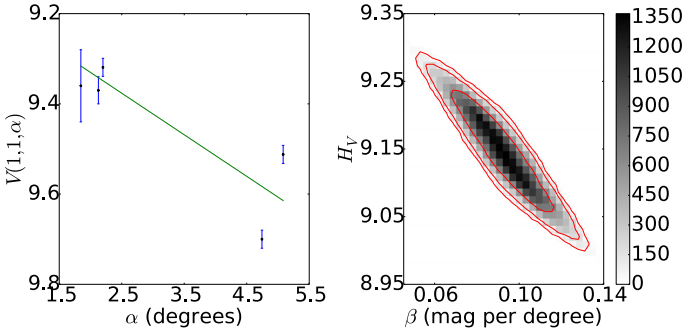

Fig. A.57. *Left*: phase curve of 120 061 2003 CO_1. The continuous line indicate the best fit to Eq. (5) resulting in $H_V = 9.146 \pm 0.056$, $\beta = (0.092 \pm 0.015)$ mag per degree. *Right*: density plot showing the phase space of solutions of Eq. (5) for $\Delta m = 0.07$, in gray scale. The continuous lines show the area that contain 68.3, 95.5, and 99.7% of the solutions.

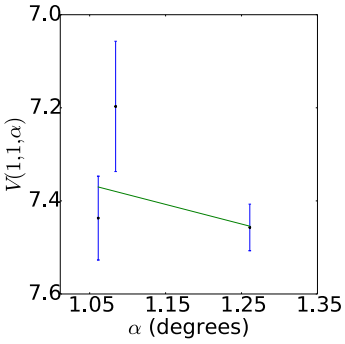

Fig. A.58. Phase curve of 133 067 2003 FB_{128}. The continuous line indicate the best fit to Eq. (5) resulting in $H_V = 6.922 \pm 0.566$, $\beta = (0.422 \pm 0.469)$ mag per degree.

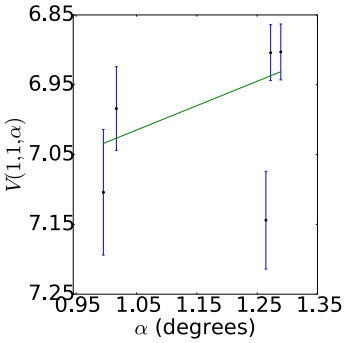

Fig. A.59. Phase curve of 2003 FE_{128}. The continuous line indicate the best fit to Eq. (5) resulting in $H_V = 7.381 \pm 0.256$, $\beta = (-0.349 \pm 0.209)$ mag per degree.

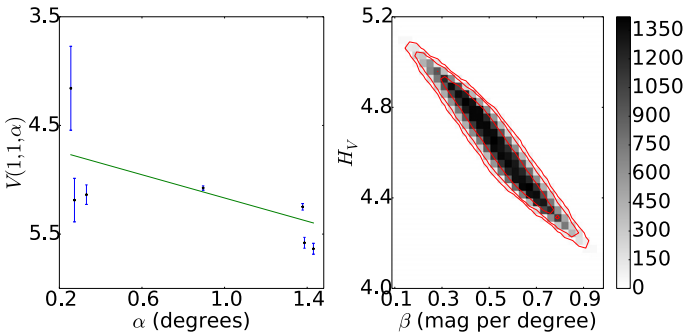

Fig. A.60. *Left*: phase curve of 120 132 2003 FY_{128}. The continuous line indicate the best fit to Eq. (5) resulting in $H_V = 4.632 \pm 0.187$, $\beta = (0.535 \pm 0.145)$ mag per degree. *Right*: density plot showing the phase space of solutions of Eq. (5) for $\Delta m = 0.15$, in gray scale. The continuous lines show the area that contain 68.3, 95.5, and 99.7% of the solutions.

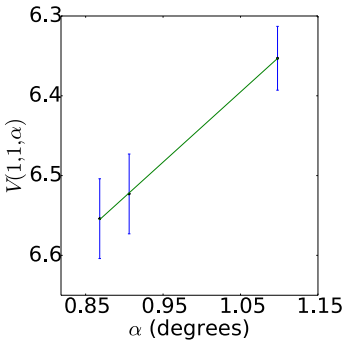

Fig. A.61. Phase curve of 385 437 2003 GH_{55}. The continuous line indicate the best fit to Eq. (5) resulting in $H_V = 7.319 \pm 0.247$, $\beta = (-0.880 \pm 0.251)$ mag per degree.

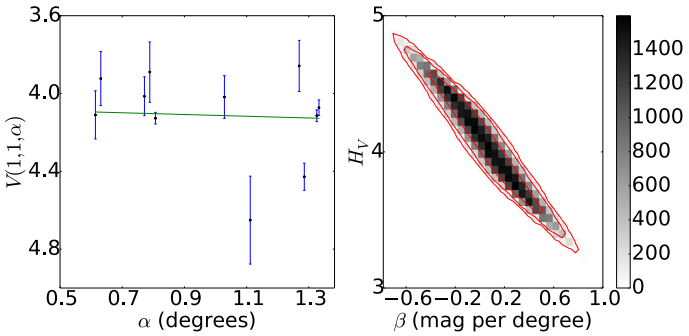

Fig. A.62. *Left*: phase curve of 120 178 2003 OP_{32}. The continuous line indicate the best fit to Eq. (5) resulting in $H_V = 4.067 \pm 0.318$, $\beta = (0.045 \pm 0.280)$ mag per degree. *Right*: density plot showing the phase space of solutions of Eq. (5) for $\Delta m = 0.26$, in gray scale. The continuous lines show the area that contain 68.3, 95.5, and 99.7% of the solutions.

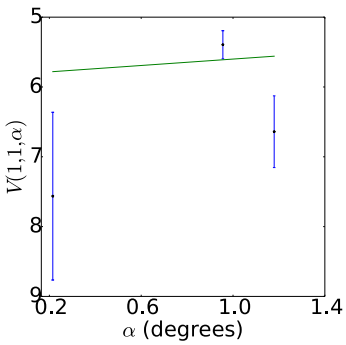

Fig. A.63. Phase curve of 143 707 2003 UY_{117}. The continuous line indicate the best fit to Eq. (5) resulting in $H_V = 5.830 \pm 1.299$, $\beta = (-0.230 \pm 1.329)$ mag per degree.

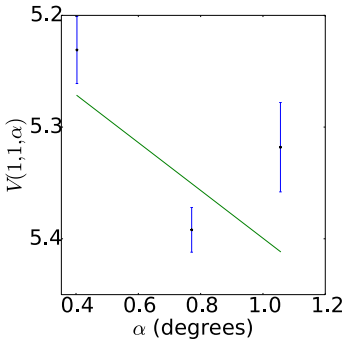

Fig. A.64. Phase curve of 2003 UZ_{117}. The continuous line indicate the best fit to Eq. (5) resulting in $H_V = 5.185 \pm 0.054$, $\beta = (0.214 \pm 0.073)$ mag per degree.

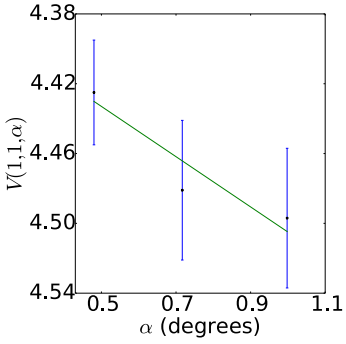

Fig. A.65. Phase curve of 2003 UZ_{413}. The continuous line indicate the best fit to Eq. (5) resulting in $H_V = 4.361 \pm 0.068$, $\beta = (0.144 \pm 0.096)$ mag per degree.

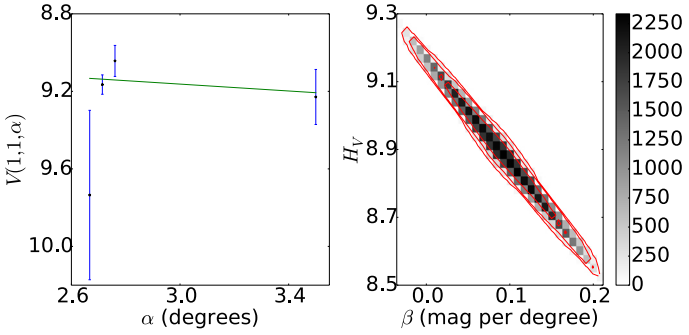

Fig. A.66. *Left*: phase curve of 136 204 2003 WL_7. The continuous line indicate the best fit to Eq. (5) resulting in $H_V = 8.897 \pm 0.149$, $\beta = (0.089 \pm 0.049)$ mag per degree. *Right*: density plot showing the phase space of solutions of Eq. (5) for $\Delta m = 0.05$, in gray scale. The continuous lines show the area that contain 68.3, 95.5, and 99.7% of the solutions.

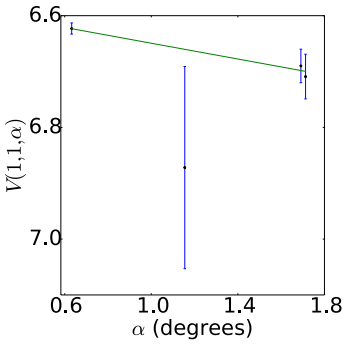

Fig. A.67. Phase curve of 120 216 2004 EW_{95}. The continuous line indicate the best fit to Eq. (5) resulting in $H_V = 6.579 \pm 0.021$, $\beta = (0.071 \pm 0.024)$ mag per degree.

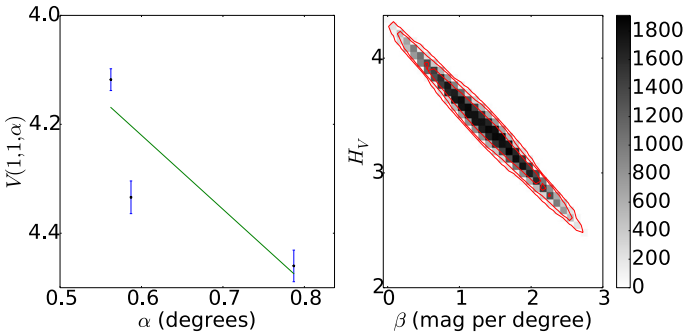

Fig. A.68. *Left*: phase curve of 90 568 2004 GV_9. The continuous line indicate the best fit to Eq. (5) resulting in $H_V = 3.409 \pm 0.357$, $\beta = (1.353 \pm 0.542)$ mag per degree. *Right*: density plot showing the phase space of solutions of Eq. (5) for $\Delta m = 0.16$, in gray scale. The continuous lines show the area that contain 68.3, 95.5, and 99.7% of the solutions.

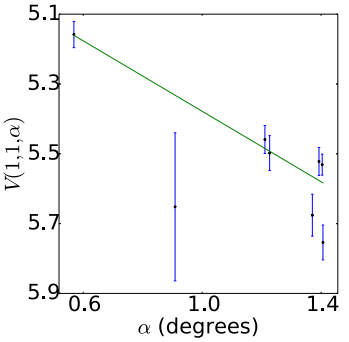

Fig. A.69. Phase curve of 307 982 2004 PG_{115}. The continuous line indicate the best fit to Eq. (5) resulting in $H_V = 4.874 \pm 0.064$, $\beta = (0.505 \pm 0.051)$ mag per degree.

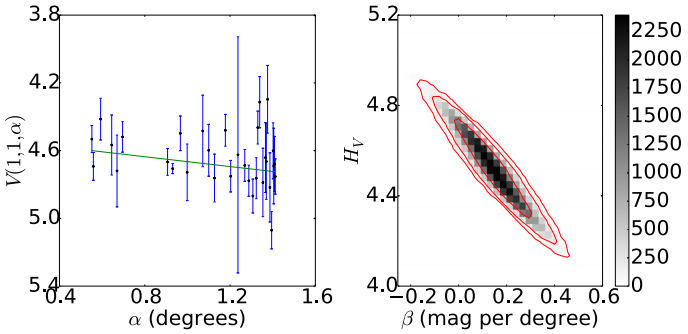

Fig. A.70. *Left*: phase curve of 120 348 2004 TY_{364}. The continuous line indicate the best fit to Eq. (5) resulting in $H_V = 4.519 \pm 0.137$, $\beta = (0.146 \pm 0.103)$ mag per degree. *Right*: density plot showing the phase space of solutions of Eq. (5) for $\Delta m = 0.22$, in gray scale. The continuous lines show the area that contain 68.3, 95.5, and 99.7% of the solutions.

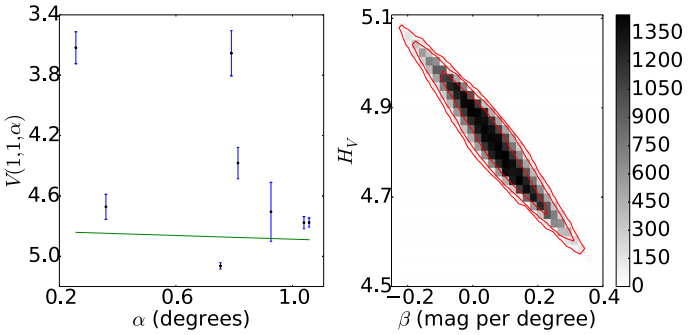

Fig. A.71. *Left*: phase curve of 144 897 2004 UX_{10}. The continuous line indicate the best fit to Eq. (5) resulting in $H_V = 4.825 \pm 0.097$, $\beta = (0.061 \pm 0.103)$ mag per degree. *Right*: density plot showing the phase space of solutions of Eq. (5) for $\Delta m = 0.08$, in gray scale. The continuous lines show the area that contain 68.3, 95.5, and 99.7% of the solutions.

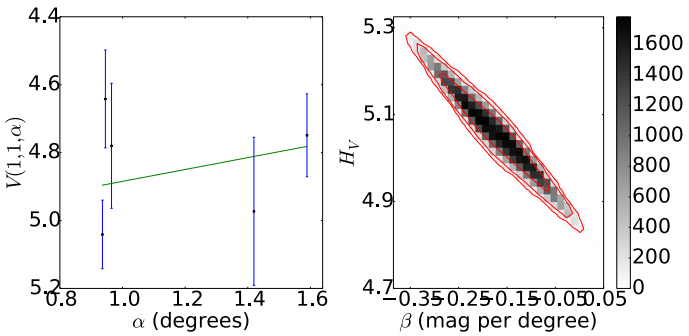

Fig. A.72. *Left*: phase curve of 230 965 2004 XA_{192}. The continuous line indicate the best fit to Eq. (5) resulting in $H_V = 5.059 \pm 0.085$, $\beta = (-0.175 \pm 0.070)$ mag per degree. *Right*: density plot showing the phase space of solutions of Eq. (5) for $\Delta m = 0.07$, in gray scale. The continuous lines show the area that contain 68.3, 95.5, and 99.7% of the solutions.

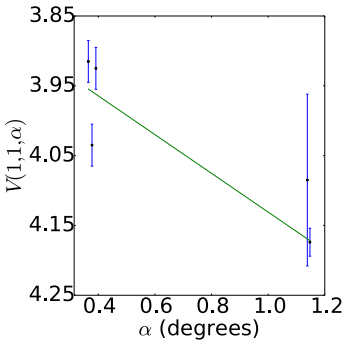

Fig. A.73. Phase curve of 303 775 2005 QU_{182}. The continuous line indicate the best fit to Eq. (5) resulting in $H_V = 3.853 \pm 0.028$, $\beta = (0.277 \pm 0.034)$ mag per degree.

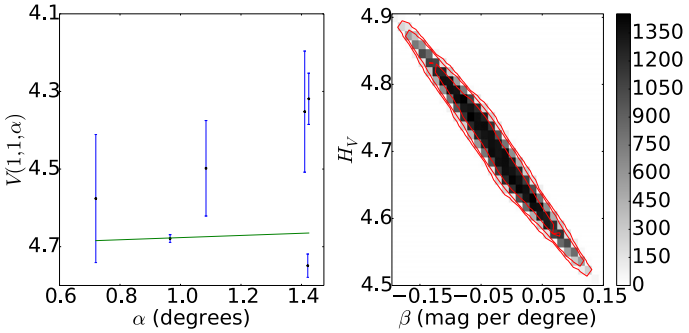

Fig. A.74. *Left*: phase curve of 145 451 2005 RM_{43}. The continuous line indicate the best fit to Eq. (5) resulting in $H_V = 4.704 \pm 0.081$, $\beta = (-0.028 \pm 0.064)$ mag per degree. *Right*: density plot showing the phase space of solutions of Eq. (5) for $\Delta m = 0.04$, in gray scale. The continuous lines show the area that contain 68.3, 95.5, and 99.7% of the solutions.

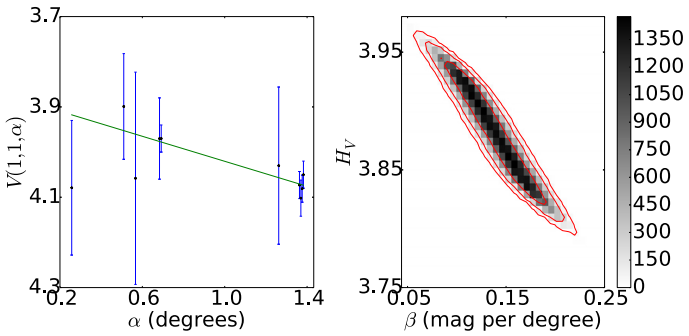

Fig. A.75. *Left*: phase curve of 145 452 2005 RN_{43}. The continuous line indicate the best fit to Eq. (5) resulting in $H_V = 3.882 \pm 0.036$, $\beta = (0.138 \pm 0.030)$ mag per degree. *Right*: density plot showing the phase space of solutions of Eq. (5) for $\Delta m = 0.04$, in gray scale. The continuous lines show the area that contain 68.3, 95.5, and 99.7% of the solutions.

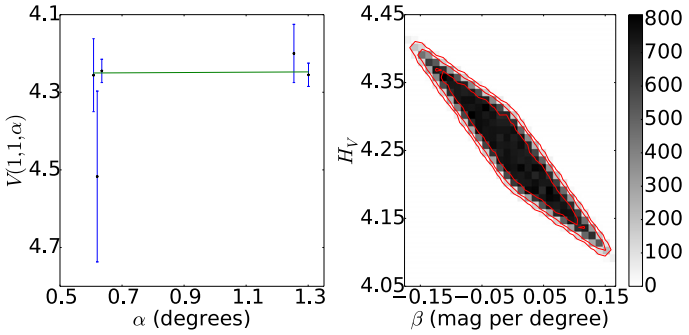

Fig. A.76. *Left*: phase curve of 145 453 2005 RR_{43}. The continuous line indicate the best fit to Eq. (5) resulting in $H_V = 4.252 \pm 0.067$, $\beta = (-0.003 \pm 0.065)$ mag per degree. *Right*: density plot showing the phase space of solutions of Eq. (5) for $\Delta m = 0.06$, in gray scale. The continuous lines show the area that contain 68.3, 95.5, and 99.7% of the solutions.

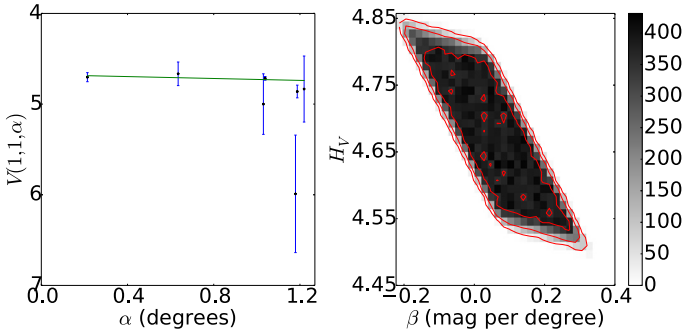

Fig. A.77. *Left*: phase curve of 145 480 2005 TB_{190}. The continuous line indicate the best fit to Eq. (5) resulting in $H_V = 4.676 \pm 0.084$, $\beta = (0.052 \pm 0.106)$ mag per degree. *Right*: density plot showing the phase space of solutions of Eq. (5) for $\Delta m = 0.12$, in gray scale. The continuous lines show the area that contain 68.3, 95.5, and 99.7% of the solutions.

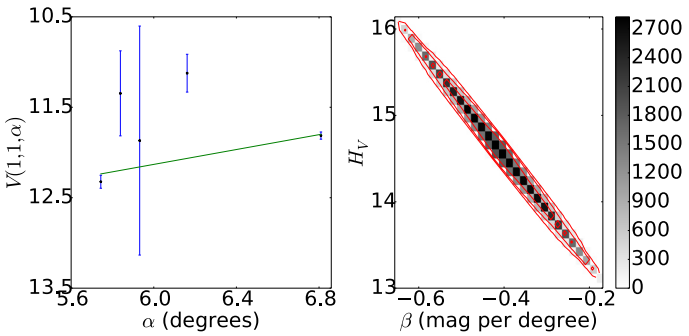

Fig. A.78. *Left*: phase curve of 145 486 2005 UJ_{438}. The continuous line indicate the best fit to Eq. (5) resulting in $H_V = 14.602 \pm 0.617$, $\beta = (-0.412 \pm 0.098)$ mag per degree. *Right*: density plot showing the phase space of solutions of Eq. (5) for $\Delta m = 0.13$, in gray scale. The continuous lines show the area that contain 68.3, 95.5, and 99.7% of the solutions.

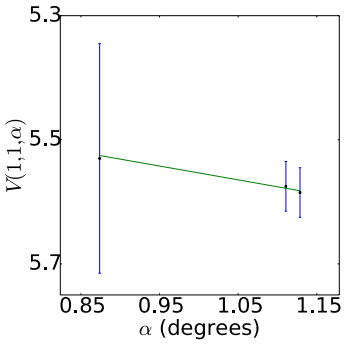

Fig. A.79. Phase curve of 2007 OC_{10}. The continuous line indicate the best fit to Eq. (5) resulting in $H_V = 5.330 \pm 0.825$, $\beta = (0.223 \pm 0.740)$ mag per degree.

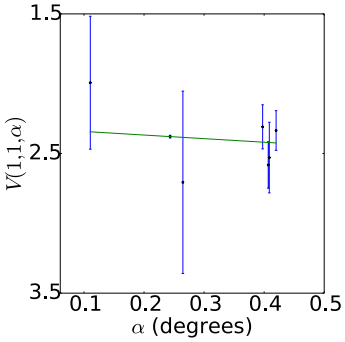

Fig. A.80. Phase curve of 225 088 2007 OR_{10}. The continuous line indicate the best fit to Eq. (5) resulting in $H_V = 2.316 \pm 0.124$, $\beta = (0.257 \pm 0.505)$ mag per degree.

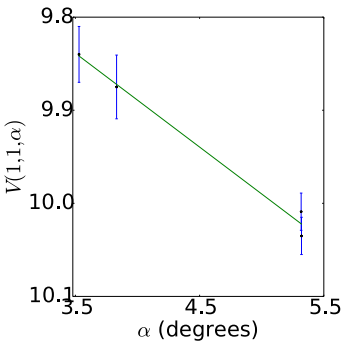

Fig. A.81. Phase curve of 281 371 2008 FC_{76}. The continuous line indicate the best fit to Eq. (5) resulting in $H_V = 9.488 \pm 0.074$, $\beta = (0.101 \pm 0.015)$ mag per degree.

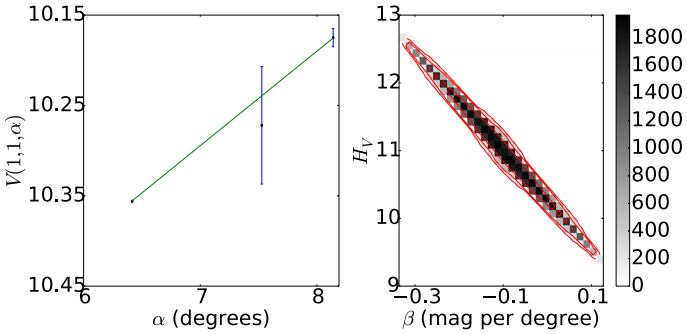

Fig. A.82. *Left*: phase curve of 342 842 2008 YB_3. The continuous line indicate the best fit to Eq. (5) resulting in $H_V = 11.024 \pm 0.696$, $\beta = (-0.104 \pm 0.095)$ mag per degree. *Right*: density plot showing the phase space of solutions of Eq. (5) for $\Delta m = 0.20$, in gray scale. The continuous lines show the area that contain 68.3, 95.5, and 99.7% of the solutions.

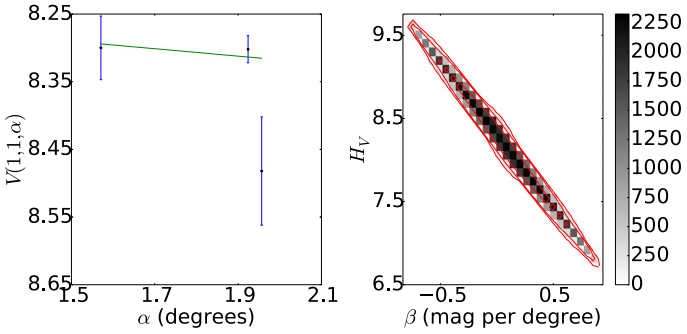

Fig. A.83. *Left*: phase curve of 55 576 Amycus. The continuous line indicate the best fit to Eq. (5) resulting in $H_V = 8.213 \pm 0.621$, $\beta = (0.052 \pm 0.351)$ mag per degree. *Right*: density plot showing the phase space of solutions of Eq. (5) for $\Delta m = 0.16$, in gray scale. The continuous lines show the area that contain 68.3, 95.5, and 99.7% of the solutions.

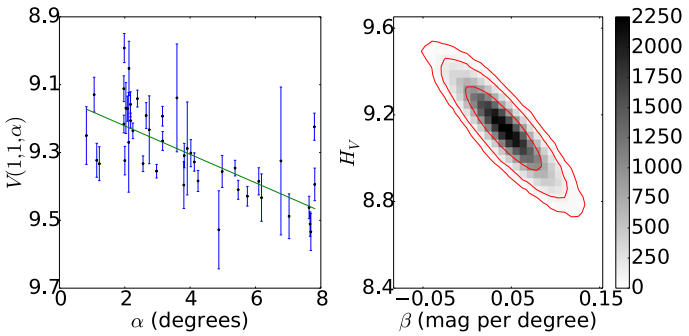

Fig. A.84. *Left*: phase curve of 8405 Asbolus. The continuous line indicate the best fit to Eq. (5) resulting in $H_V = 9.138 \pm 0.130$, $\beta = (0.042 \pm 0.029)$ mag per degree. *Right*: density plot showing the phase space of solutions of Eq. (5) for $\Delta m = 0.55$, in gray scale. The continuous lines show the area that contain 68.3, 95.5, and 99.7% of the solutions.

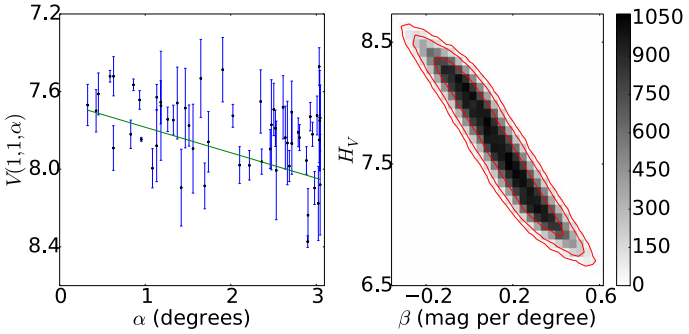

Fig. A.85. *Left*: phase curve of 54 598 Bienor. The continuous line indicate the best fit to Eq. (5) resulting in $H_V = 7.656 \pm 0.443$, $\beta = (0.130 \pm 0.170)$ mag per degree. *Right*: density plot showing the phase space of solutions of Eq. (5) for $\Delta m = 0.75$, in gray scale. The continuous lines show the area that contain 68.3, 95.5, and 99.7% of the solutions.

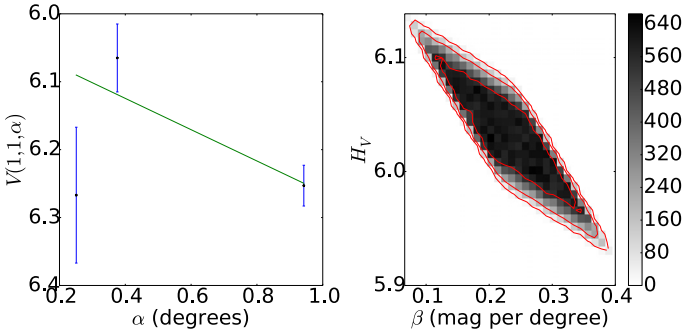

Fig. A.86. *Left*: phase curve of 66 652 Borasisi. The continuous line indicate the best fit to Eq. (5) resulting in $H_V = 6.032 \pm 0.040$, $\beta = (0.231 \pm 0.062)$ mag per degree. *Right*: density plot showing the phase space of solutions of Eq. (5) for $\Delta m = 0.05$, in gray scale. The continuous lines show the area that contain 68.3, 95.5, and 99.7% of the solutions.

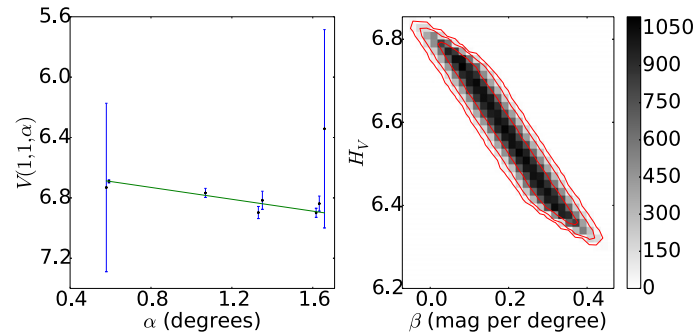

Fig. A.87. *Left*: phase curve of 65 489 Ceto. The continuous line indicate the best fit to Eq. (5) resulting in $H_V = 6.573 \pm 0.126$, $\beta = (0.196 \pm 0.096)$ mag per degree. *Right*: density plot showing the phase space of solutions of Eq. (5) for $\Delta m = 0.13$, in gray scale. The continuous lines show the area that contain 68.3, 95.5, and 99.7% of the solutions.

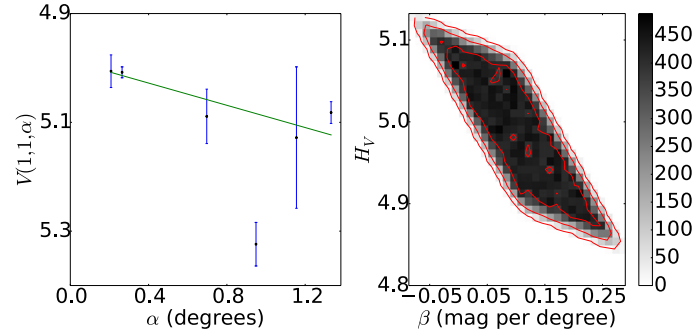

Fig. A.88. *Left*: phase curve of 19521 Chaos. The continuous line indicate the best fit to Eq. (5) resulting in $H_V = 4.987 \pm 0.065$, $\beta = (0.102 \pm 0.070)$ mag per degree. *Right*: density plot showing the phase space of solutions of Eq. (5) for $\Delta m = 0.10$, in gray scale. The continuous lines show the area that contain 68.3, 95.5, and 99.7% of the solutions.

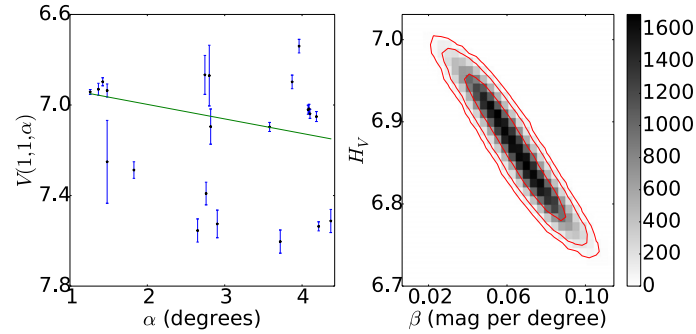

Fig. A.89. *Left*: phase curve of 10 199 Chariklo. The continuous line indicate the best fit to Eq. (5) resulting in $H_V = 6.870 \pm 0.055$, $\beta = (0.064 \pm 0.016)$ mag per degree. *Right*: density plot showing the phase space of solutions of Eq. (5) for $\Delta m = 0.10$, in gray scale. The continuous lines show the area that contain 68.3, 95.5, and 99.7% of the solutions.

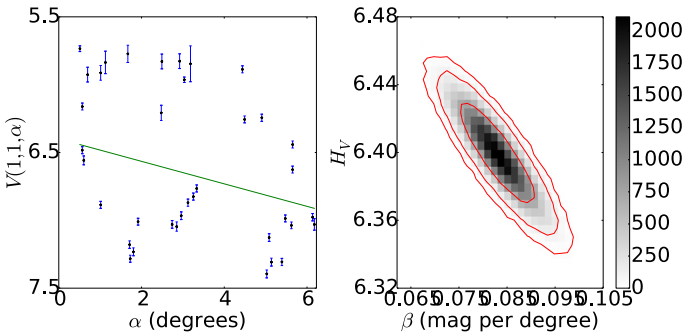

Fig. A.90. *Left*: phase curve of 2060 Chiron. The continuous line indicate the best fit to Eq. (5) resulting in $H_V = 6.399 \pm 0.019$, $\beta = (0.083 \pm 0.005)$ mag per degree. *Right*: density plot showing the phase space of solutions of Eq. (5) for $\Delta m = 0.09$, in gray scale. The continuous lines show the area that contain 68.3, 95.5, and 99.7% of the solutions.

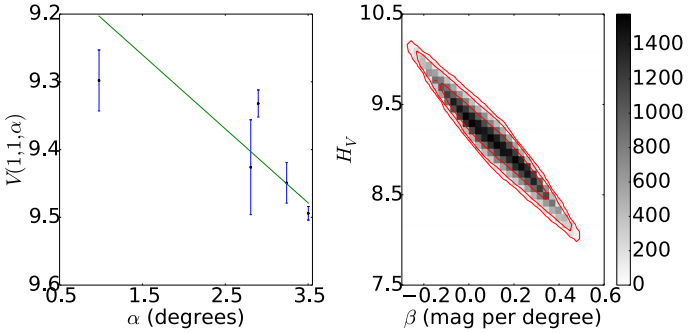

Fig. A.91. *Left*: phase curve of 83982 Crantor. The continuous line indicate the best fit to Eq. (5) resulting in $H_V = 9.096 \pm 0.405$, $\beta = (0.110 \pm 0.149)$ mag per degree. *Right*: density plot showing the phase space of solutions of Eq. (5) for $\Delta m = 0.34$, in gray scale. The continuous lines show the area that contain 68.3, 95.5, and 99.7% of the solutions.

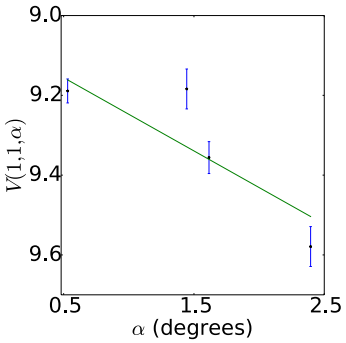

Fig. A.92. Phase curve of 52 975 Cyllarus. The continuous line indicate the best fit to Eq. (5) resulting in $H_V = 9.064 \pm 0.041$, $\beta = (0.184 \pm 0.029)$ mag per degree.

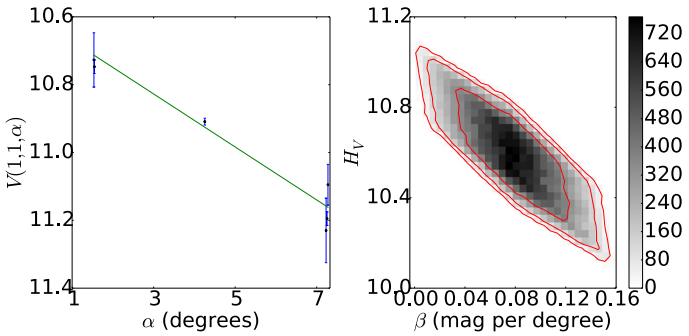

Fig. A.93. *Left*: phase curve of 31 824 Elatus. The continuous line indicate the best fit to Eq. (5) resulting in $H_V = 10.592 \pm 0.171$, $\beta = (0.078 \pm 0.031)$ mag per degree. *Right*: density plot showing the phase space of solutions of Eq. (5) for $\Delta m = 0.24$, in gray scale. The continuous lines show the area that contain 68.3, 95.5, and 99.7% of the solutions.

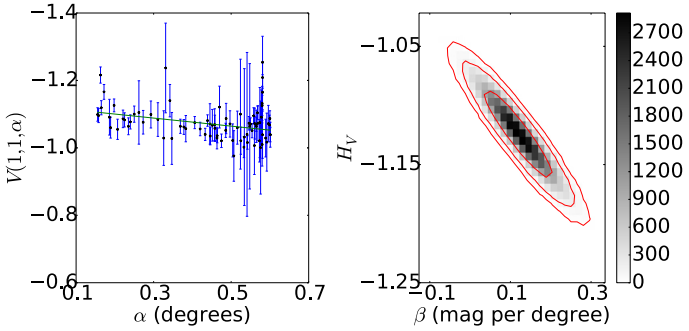

Fig. A.94. *Left*: phase curve of 136 199 Eris. The continuous line indicate the best fit to Eq. (5) resulting in $H_V = -1.124 \pm 0.025$, $\beta = (0.119 \pm 0.056)$ mag per degree. *Right*: density plot showing the phase space of solutions of Eq. (5) for $\Delta m = 0.10$, in gray scale. The continuous lines show the area that contain 68.3, 95.5, and 99.7% of the solutions.

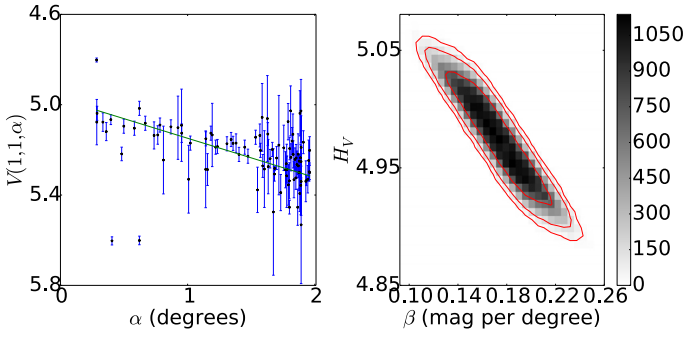

Fig. A.95. *Left*: phase curve of 38 628 Huya. The continuous line indicate the best fit to Eq. (5) resulting in $H_V = 4.975 \pm 0.037$, $\beta = (0.173 \pm 0.026)$ mag per degree. *Right*: density plot showing the phase space of solutions of Eq. (5) for $\Delta m = 0.10$, in gray scale. The continuous lines show the area that contain 68.3, 95.5, and 99.7% of the solutions.

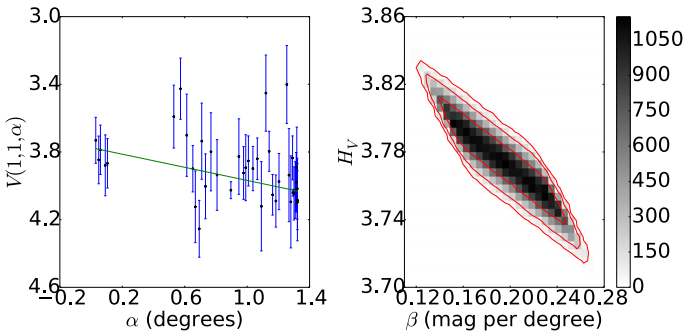

Fig. A.96. *Left*: phase curve of 28978 Ixion. The continuous line indicate the best fit to Eq. (5) resulting in $H_V = 3.774 \pm 0.021$, $\beta = (0.194 \pm 0.031)$ mag per degree. *Right*: density plot showing the phase space of solutions of Eq. (5) for $\Delta m = 0.05$, in gray scale. The continuous lines show the area that contain 68.3, 95.5, and 99.7% of the solutions.

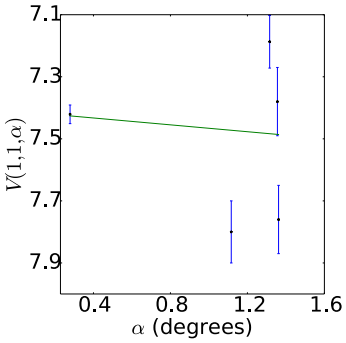

Fig. A.97. Phase curve of 58534 Logos. The continuous line indicate the best fit to Eq. (5) resulting in $H_V = 7.411 \pm 0.041$, $\beta = (0.055 \pm 0.057)$ mag per degree.

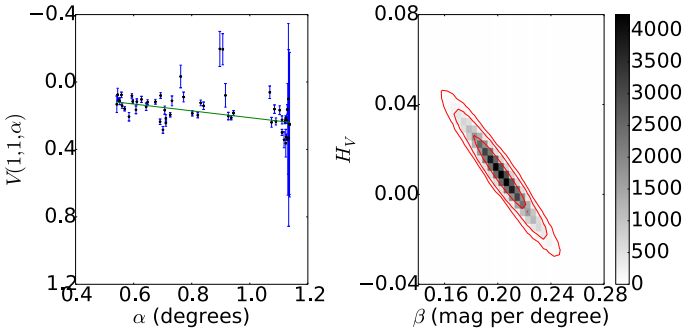

Fig. A.98. *Left*: phase curve of 136472 Makemake. The continuous line indicate the best fit to Eq. (5) resulting in $H_V = 0.009 \pm 0.012$, $\beta = (0.202 \pm 0.015)$ mag per degree. *Right*: density plot showing the phase space of solutions of Eq. (5) for $\Delta m = 0.03$, in gray scale. The continuous lines show the area that contain 68.3, 95.5, and 99.7% of the solutions.

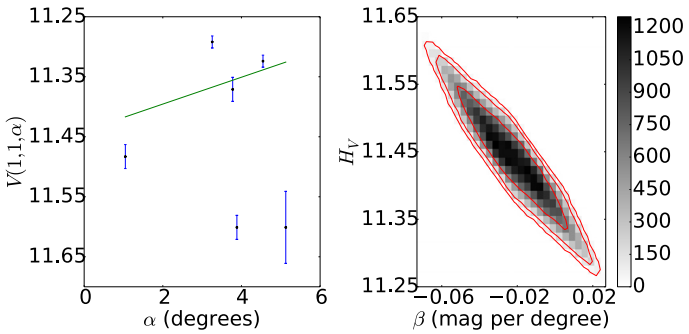

Fig. A.99. *Left*: phase curve of 52 872 Okyrhoe. The continuous line indicate the best fit to Eq. (5) resulting in $H_V = 11.441 \pm 0.062$, $\beta = (-0.023 \pm 0.017)$ mag per degree. *Right*: density plot showing the phase space of solutions of Eq. (5) for $\Delta m = 0.07$, in gray scale. The continuous lines show the area that contain 68.3, 95.5, and 99.7% of the solutions.

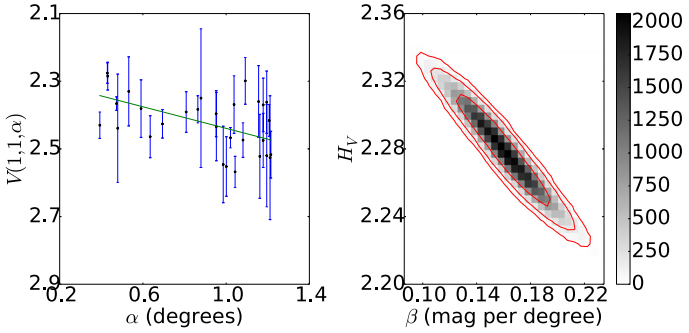

Fig. A.100. *Left*: phase curve of 90 482 Orcus. The continuous line indicate the best fit to Eq. (5) resulting in $H_V = 2.280 \pm 0.021$, $\beta = (0.160 \pm 0.022)$ mag per degree. *Right*: density plot showing the phase space of solutions of Eq. (5) for $\Delta m = 0.04$, in gray scale. The continuous lines show the area that contain 68.3, 95.5, and 99.7% of the solutions.

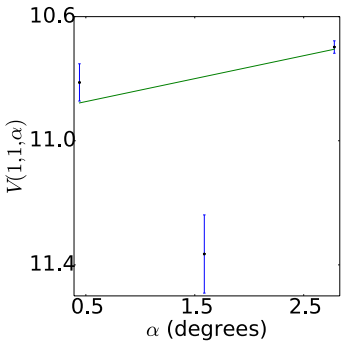

Fig. A.101. Phase curve of 49 036 Pelion. The continuous line indicate the best fit to Eq. (5) resulting in $H_V = 10.911 \pm 0.069$, $\beta = (-0.074 \pm 0.026)$ mag per degree.

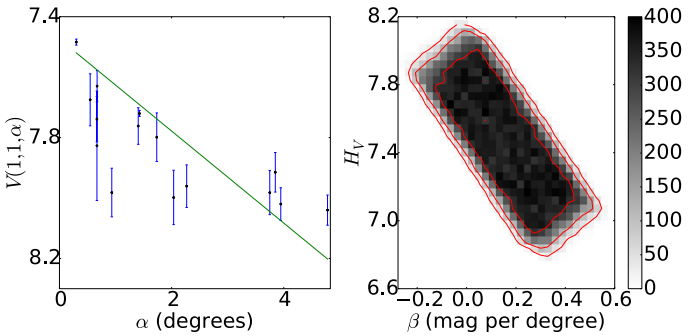

Fig. A.102. *Left*: phase curve of 5145 Pholus. The continuous line indicate the best fit to Eq. (5) resulting in $H_V = 7.474 \pm 0.309$, $\beta = (0.153 \pm 0.156)$ mag per degree. *Right*: density plot showing the phase space of solutions of Eq. (5) for $\Delta m = 0.60$, in gray scale. The continuous lines show the area that contain 68.3, 95.5, and 99.7% of the solutions.

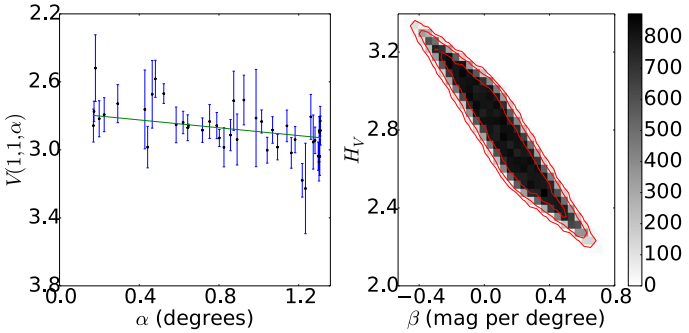

Fig. A.103. *Left*: phase curve of 50 000 Quaoar. The continuous line indicate the best fit to Eq. (5) resulting in $H_V = 2.777 \pm 0.250$, $\beta = (0.117 \pm 0.221)$ mag per degree. *Right*: density plot showing the phase space of solutions of Eq. (5) for $\Delta m = 0.30$, in gray scale. The continuous lines show the area that contain 68.3, 95.5, and 99.7% of the solutions.

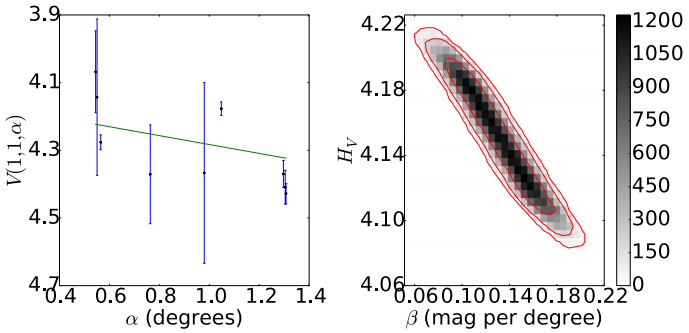

Fig. A.104. *Left*: phase curve of 120347 Salacia. The continuous line indicate the best fit to Eq. (5) resulting in $H_V = 4.151 \pm 0.030$, $\beta = (0.132 \pm 0.028)$ mag per degree. *Right*: density plot showing the phase space of solutions of Eq. (5) for $\Delta m = 0.03$, in gray scale. The continuous lines show the area that contain 68.3, 95.5, and 99.7% of the solutions.

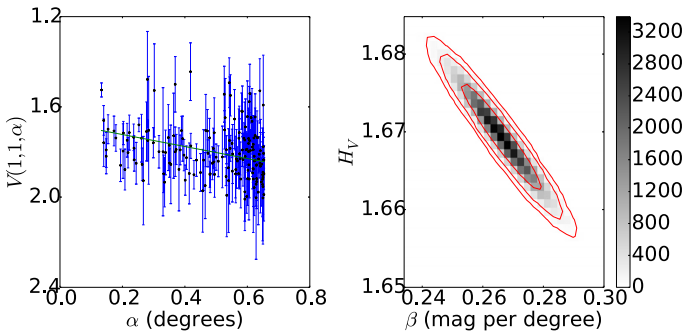

Fig. A.105. *Left*: phase curve of 90377 Sedna. The continuous line indicate the best fit to Eq. (5) resulting in $H_V = 1.669 \pm 0.004$, $\beta = (0.266 \pm 0.008)$ mag per degree. *Right*: density plot showing the phase space of solutions of Eq. (5) for $\Delta m = 0.02$, in gray scale. The continuous lines show the area that contain 68.3, 95.5, and 99.7% of the solutions.

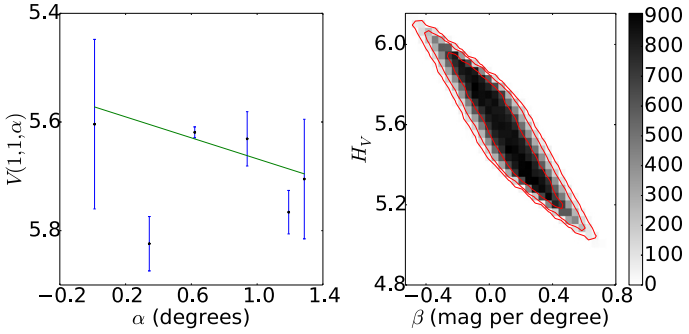

Fig. A.106. *Left*: phase curve of 79360 Sila-Numan. The continuous line indicate the best fit to Eq. (5) resulting in $H_V = 5.573 \pm 0.224$, $\beta = (0.095 \pm 0.209)$ mag per degree. *Right*: density plot showing the phase space of solutions of Eq. (5) for $\Delta m = 0.22$, in gray scale. The continuous lines show the area that contain 68.3, 95.5, and 99.7% of the solutions.

Fig. A.107. *Left*: phase curve of 32532 Thereus. The continuous line indicate the best fit to Eq. (5) resulting in $H_V = 9.454 \pm 0.137$, $\beta = (0.061 \pm 0.034)$ mag per degree. *Right*: density plot showing the phase space of solutions of Eq. (5) for $\Delta m = 0.34$, in gray scale. The continuous lines show the area that contain 68.3, 95.5, and 99.7% of the solutions.

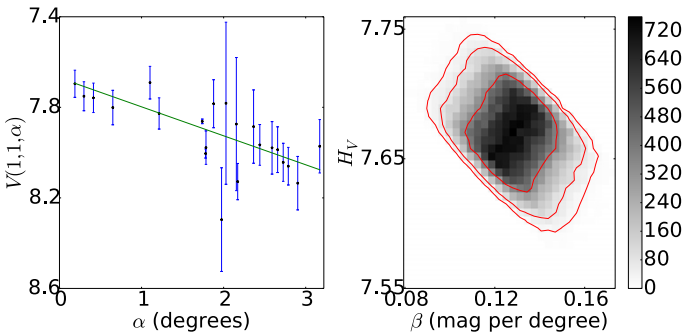

Fig. A.108. *Left*: phase curve of 42355 Typhon. The continuous line indicate the best fit to Eq. (5) resulting in $H_V = 7.670 \pm 0.026$, $\beta = (0.128 \pm 0.013)$ mag per degree. *Right*: density plot showing the phase space of solutions of Eq. (5) for $\Delta m = 0.07$, in gray scale. The continuous lines show the area that contain 68.3, 95.5, and 99.7% of the solutions.

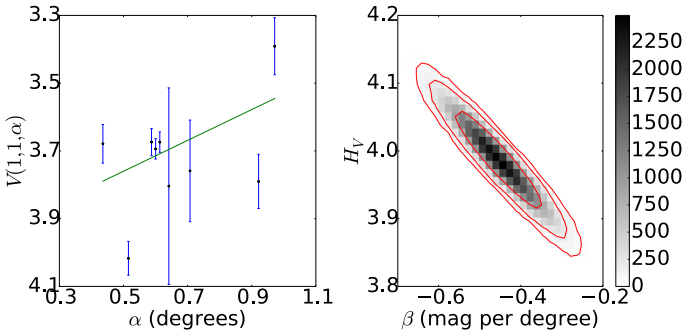

Fig. A.109. *Left*: phase curve of 174567 Varda. The continuous line indicate the best fit to Eq. (5) resulting in $H_V = 3.988 \pm 0.048$, $\beta = (-0.455 \pm 0.071)$ mag per degree. *Right*: density plot showing the phase space of solutions of Eq. (5) for $\Delta m = 0.06$, in gray scale. The continuous lines show the area that contain 68.3, 95.5, and 99.7% of the solutions.

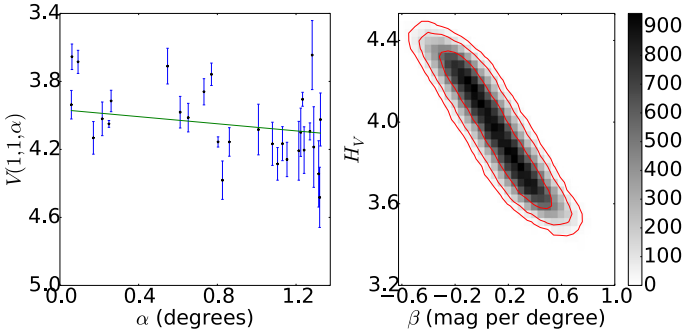

Fig. A.110. *Left*: phase curve of 20 000 Varuna. The continuous line indicate the best fit to Eq. (5) resulting in $H_V = 3.966 \pm 0.233$, $\beta = (0.104 \pm 0.246)$ mag per degree. *Right*: density plot showing the phase space of solutions of Eq. (5) for $\Delta m = 0.50$, in gray scale. The continuous lines show the area that contain 68.3, 95.5, and 99.7% of the solutions.